

# Carbon Capture in Pulp Mills: Modelling and Process Integration Strategies

Master's Thesis

By

Enzo Robano Suárez

Department of Energy Sciences  
Faculty of Engineering, LTH, Lund University  
June 2024



**LUND UNIVERSITY**

Supervisor: Hesam Fatehi, Lund University  
Co-supervisor: Joonas Alaraudanjoki, Stora Enso  
Examiner: Jens Klingmann, Lund University



## Abstract

The bioenergy industry, particularly pulp mills, holds promise for achieving carbon negativity through the adoption of carbon capture processes. Presently, CO<sub>2</sub> capture from flue gases poses significant challenges due to its energy-intensive nature and the risk of solvent chemical degradation.

This thesis conducts a screening of primary absorption technologies and models a carbon capture process in a stand-alone pulp mill. The modeling is executed using Aspen Plus, followed by a process integration study to identify energy source alternatives within the mill while minimizing steam usage.

The model indicates a requirement of 3.6 MJ/kgCO<sub>2</sub> for capture, with a feasible energy supply strategy involving the integration of a low-pressure steam generation heat pump to utilize waste hot water streams within the mill. Additionally, alternatives such as incorporating a new combustion air preheater have been explored, showcasing potential electricity savings of up to 3,5 MW, although with marginal reductions in steam flow for carbon capture applications.

In conclusion, first implementing carbon capture in the lime kiln is recommended due to its smaller column size and lower energy demand compared to the recovery boiler. Furthermore, conducting a more exhaustive energy efficiency assessment of the mill is advised to identify additional sources of waste heat usable by the heat pump.

## Acknowledgment

I would like to express my sincere gratitude to Hesam and Joonas, both supervisors from Lund University and Stora Enso, for their invaluable guidance, support, and insightful contributions throughout the development of this thesis.

Additionally, I extend my thanks to Sarah, Maria, and Dan from Stora Enso for kindly opening the doors of the company and providing me with the opportunity to undertake this thesis project with their organization.

Lastly, I am deeply grateful to my former colleagues at Montes del Plata for their support and continuous communication. Petri, Enrique, and Marko, your assistance has been key in the completion of this thesis. Thank you very much for your collaboration and dedication.

## Nomenclature

Adt: Air dry tonne  
BL: Black Liquor  
CC: Carbon capture  
COP: Coefficient of performance  
FGC: Flue gas cooler  
FG: Flue gas  
HPC: Hot Potassium Carbonate  
HP: Heat Pump  
HPS: High-Pressure Steam  
HTHP: High-Temperature Heat Pump  
HW: Hot Water  
LK: Lime Kiln  
LPS: Low-Pressure Steam  
MdP: Montes del Plata  
MEA: Mono-ethanol-amine  
MPS: Medium Pressure Steam  
PB: Power Boiler  
RB: Recovery Boiler  
SGHP: Steam Generation Heat Pump  
TG: Turbine Generator  
TRL: Technology readiness level  
WW: Warm Water

## Table of Contents

Abstract.....	II
Nomenclature.....	IV
1 Introduction .....	1
1.1 The potential of CO <sub>2</sub> as a sub-product.....	2
1.2 CO <sub>2</sub> capture technologies overview .....	4
1.2.1 Adsorption.....	5
1.2.2 Membranes .....	5
1.2.3 Cryogenic separation.....	5
2 Main absorption CO <sub>2</sub> process .....	5
2.1 Amine-based solvents.....	6
2.1.1 MEA .....	6
2.1.2 AMP/DMSO .....	7
2.2 Carbonate-based solvent.....	8
2.2.1 HPC (Hot Potassium Carbonate) .....	9
2.3 Enzyme absorption carbon capture .....	9
2.4 Summary of the chemical absorption technologies .....	10
2.5 Motivation for choosing the amine-based carbon capture module .....	11
3 Pulp mill basic operation description.....	12
3.1 Steam cycle in a stand-alone mill .....	13
3.2 Warm and Hot water production .....	14
4 Literature review.....	14
5 MEA CC in Aspen Plus: Modeling, calibration, and validation.....	15
5.1 Columns modeling: Mass and energy balances.....	16
5.1.1 Mass and energy balance: Bulk liquid and gaseous phases.....	17
5.1.1 Mass and energy balance: Interphase.....	18
5.2 Columns modeling: Chemical reactions .....	20
5.3 Columns modeling: Profiles and transfer coefficients.....	22
5.4 Columns modeling: Geometrical and operational parameters.....	22
5.5 Modeling the external components .....	23
5.6 Kinetic parameters selection.....	23
5.7 Absorber validation.....	25
5.8 Stripper Validation .....	27
6 Results .....	28
6.1 Standard MEA CC for the RB.....	29
6.1.1 Absorber model for the RB .....	29
6.1.2 Stripper model for the RB.....	33
6.1.3 MEA Cycle model for the RB .....	35
6.1.4 Sensitivity analysis for the RB: Variation of the capture efficiency.....	36

6.1.5	Sensitivity analysis for the RB: Variation of stripper inlet temperature .....	37
6.1.6	Sensitivity analysis for the RB: Variation of stripper operation pressure .....	38
6.2	Final MEA process for the RB .....	39
6.3	Final MEA process for the LK .....	40
6.4	Impact of CC in the mill .....	40
7	Process integration study.....	42
7.1	Use flue gas (FG) in CC .....	43
7.2	Heat pumps for hot and warm water streams .....	44
7.3	Hot water (HW) to preheat combustion air in the RB.....	47
7.4	Summary .....	49
8	Conclusions .....	49
9	References.....	51

# 1 Introduction

Reducing greenhouse gas emissions is a major concern worldwide as highlighted by the urgent goal set by the IPCC (Intergovernmental Panel on Climate Change) in the Global Warming Report to limit temperature rise to 1.5°C by 2050 through transitioning to cleaner energy sources (IPCC, 2022). Industry emissions accounted for around 9,5 Gt of CO<sub>2</sub> in a total of 34,74 Gt of CO<sub>2</sub> in 2022. Furthermore, the industry sector is mainly dependent on fossil fuels, accounting for around 65% of the energy source spectrum (IEA, 2023a).

In general, the industry sector (steel, cement, chemical) is difficult to decarbonize because of the dependence on high-temperature processes (IEA, 2023a). At the same time, the consumption of these products will tend to increase, due to the increasing population (IEA, 2023a). Distinguished from the other industries, the pulp and paper sector has the advantage of using renewable raw materials as biomass for mainly all the processes. Despite that, according to the International Energy Agency's 2023 report, the pulp and paper sector accounts for 2% of global CO<sub>2</sub> emissions in the industrial sector (IEA, 2023b)

The Bioenergy sector with and without carbon capture, plays an important role in the pathways presented in the IPCC report for limiting the temperature rise to 1,5°C (IPCC, 2022). Although debatable, pulp mills have from the nature of their raw material, the potential to become a carbon-negative industry by the implementation of Carbon Capture and Storage (CCS) technologies (Svensson et al., 2021). In the IEA (International Energy Agency) Sustainable Development Scenario, the CO<sub>2</sub> capture capacity in the industry sector should be 423 Mt CO<sub>2</sub> by 2030 (IEA, 2020). A modern pulp mill in South America emits, around 3 Mt CO<sub>2</sub>/year (Kuparinen et al., 2019), which means that 157 modern pulp mills should implement CC if all that CO<sub>2</sub> is meant to be captured only from pulp and paper industries.

Additionally, due to the importance of bioenergy in the energy and industry transition, the CO<sub>2</sub> market is growing (Finance, 2024). The EU (European Union) is founding and promoting carbon management in the industry sector mainly through three programs, Horizon Europe, where low technology readiness level (TRL) projects are promoted. The Innovation Fund supports high TRL projects to see their viability. Finally, the Connecting Europe Facility looks at the deployment of the CO<sub>2</sub> value chain by the construction of CO<sub>2</sub> cross-border infrastructure and commercialization of technologies (Agency, 2024).

Several approved projects for the implementation of CC in the Cement industry will be in operation in around 2027 (Agency, 2024). Nowadays, there are 21 commercial-scale CCs in Europe. However, only one project is in for the pulp industry, whereas around 5 projects are associated with bioenergy CC (Agency, 2024). With the market growing, multiple companies and institutions are developing products and technologies for carbon capture, focusing mainly on reducing energy consumption and operational costs (Barlow et al., 2023).

Having presented the importance of CC in the industry and how its implementation in bioenergy and pulp and paper industry is being delayed, compared with other sectors. This thesis aims to answer the following questions:

- How much energy is needed for capturing the CO<sub>2</sub> from a modern pulp mill?
- Where can that energy be taken from with a minimal impact on the mill's energy injection to the grid?

A study case of a pulp mill in Uruguay will be used during this study. Montes del Plata (MdP) is a pulp mill in Uruguay, where Stora Enso has a joint venture contract with another Chilean forest company, Arauco. MdP has been chosen for being a modern mill (operation since 2014) and back then it was one of the biggest in the world (lab-ndt, 2014). Furthermore, another reason chosen MdP is that in Uruguay an e-fuel production project has been approved, where the CO<sub>2</sub> will be captured from a bioethanol plant and will be blended with the green hydrogen (Uruguay XXI, 2023). From now, MdP pulp mill will be referred to as, “the mill”, understanding that it is the only pulp mill that will be mentioned in this study.

To answer the research questions (RQs), three main studies will be performed. The first one, is more theoretical, where the main CC technologies will be described, in general terms and market trends. Secondly, one CC technology will be modeled in Aspen Plus and validated against experimental data from pilot plants, this will answer the first RQ. Finally, a process integration study will be performed, specifically with the MdP case and what can be done to implement CC with the lowest energy impact possible.

### 1.1 The potential of CO<sub>2</sub> as a sub-product

Carbon dioxide is the raw material in many applications, the main three are in the manufacture of fertilizers, in the oil and gas industry, and finally in the food and beverage industry. The production of synthetic fuels is in a less developed stage but with high interest due to the possibility of transport decarbonization while utilizing the same combustion technology (IEA, 2019).

Uruguay is in its “second energy transition” project and has announced it is interested in green hydrogen production, where the project bases are mentioned in the Green Hydrogen Roadmap (MIEM, 2022). As can be seen in Figure 1 the second energy transition is divided into 3 phases where in all the phases, there is expected to be an increase in production and demand of Hydrogen and synthetic fuels. The production of green H<sub>2</sub> will open the market for the production of synthetic fuel and green ammonia, which can further be used for the production of green urea (fertilizer) (Bastarrica Anselmi et al., 2023).

<b>Roadmap phases</b>	<b>Phase 1 (2022 - 2025):</b> Develop regulation; develop first pilot projects; attract first export-scale projects.	<b>Phase 2 (2026 - 2030):</b> Domestic expansion; start of the first export-scale projects.	<b>Phase 3 (+2030):</b> Large-scale domestic market; accelerated growth of exports.
Project overview	+1-2 small-scale projects implemented, larger-scale projects under development.	+3-4 medium-scale projects (100-200 MW) and +1-2 scaled projects.	+ medium-scale projects (100-200 MW) and + larger-scale projects.
<b>Production</b> (energy and hydrogen production)	<ul style="list-style-type: none"> <li>● 200-500 MW of RES power capacity under development.</li> <li>● ~50 MW of H<sub>2</sub> production capacity for small scale and 100-300 MW under development.</li> </ul>	<ul style="list-style-type: none"> <li>● 2-4 GW of RES feed-in capacity.</li> <li>● 1-2 GW of H<sub>2</sub> production capacity.</li> </ul>	<ul style="list-style-type: none"> <li>● ~20 GW of RES capacity.</li> <li>● ~10 GW of H<sub>2</sub> and derivatives production capacity.</li> </ul>
<b>Demand</b> (end uses in mobility, industry, and energy)	<ul style="list-style-type: none"> <li>● +1-2 small-scale projects implemented for transportation uses (heavy trucks, long-distance buses, agricultural vehicles).</li> <li>● +1 project under development in synfuels (incl. methanol).</li> </ul>	<ul style="list-style-type: none"> <li>● ~1-2 scaled projects under development for synfuels.</li> <li>● +domestic transport projects; H<sub>2</sub> derivatives projects for maritime transport or fertilizers.</li> </ul>	<ul style="list-style-type: none"> <li>● ~3-4 scaled projects under development for synfuel, H<sub>2</sub> and NH<sub>3</sub> exports.</li> <li>● More domestic projects throughout sectors (e.g., transportation, shipping, fertilizers, etc.).</li> </ul>
<b>Infrastructure and logistics</b> (pipelines, storage, ports)	<ul style="list-style-type: none"> <li>● Plan and develop detailed engineering for pipelines, transmission lines and ports.</li> <li>● Develop port solution for synfuels export in Montevideo.</li> </ul>	<ul style="list-style-type: none"> <li>● Plan and develop detailed engineering for Atlantic export ports.</li> <li>● Implement infrastructure plan (i.e., pipelines and transmission lines) and orchestrate coordinated deployment to capture synergies.</li> </ul>	<ul style="list-style-type: none"> <li>● Build logistics solution for export by coastal zone in the East.</li> <li>● Continue orchestrated coordination of infrastructure deployment to capture synergies.</li> </ul>

Figure 1: Green Hydrogen Roadmap (MIEM,2022)

Based on the green hydrogen production roadmap the production of e-methanol and e-jet fuel is projected to increase in the coming years. Recently the second energy transition of the country has moved into phase 2 and a project of 0,18 Million Ton e-methanol/year has been approved, which will require 0,71 Million Ton CO<sub>2</sub>/year and 0.1Million Ton H<sub>2</sub>/year (Stipanovic, 2023). In phase 2, the installation of 2 GW of renewable energy has been approved. However, for phase 3, the production of green hydrogen and derivatives is expected to require 20 GW of renewable energy to produce 10 GW of H<sub>2</sub> and derivatives.

The total biogenic CO<sub>2</sub> in Uruguay is 11,3 Million Ton/year (Vukasovic and Messina, 2023), and the three pulp mills in Uruguay account for 9,36 Million Ton/year where Mdp represents around 33% of that.

Due to the high expected H<sub>2</sub> and derivatives production in phase 3 of the project and the high share of biogenic CO<sub>2</sub> of the pulp mills, it is reasonable to think that the CO<sub>2</sub> from the pulp mills will be a valuable commodity in the future. Additionally, the location of Mdp, with a direct sea connection makes the mill an excellent hub for synthetic fuel production, and looking forward to exportation as is planned in phase 3.

The 10 GW of H<sub>2</sub> and derivatives project in phase 3 (2040) are composed of e-methanol, e-jet fuel, pure H<sub>2</sub>, and ammonia (MIEM, 2022). Assuming that 10% of the total production is considered to be e-methanol, considering an LHV of 19,9 MJ/kg the production will be 50,25 Kg/s, and considering a value of 1,43 KgCO<sub>2</sub>/KgMeOH (Vukasovic and Messina, 2023) the amount of CO<sub>2</sub> needed will be 71,8 Kg/s. Part of that amount (22,5 Kg/s) will be already supplied by the CO<sub>2</sub> capture project in another biogenic source, Alur (Stipanovic, 2023) so the other 49,35 Kg/s needs to be supplied from one of the pulp mills.

This estimation of CO<sub>2</sub> demand in phase 3 is only for e-methanol production (domestic and exportation). This has been a conservative estimation, because as can be seen in Figure 2 there will also be an exportation of synthetic jet fuel, meaning that the CO<sub>2</sub> needed will also increase.

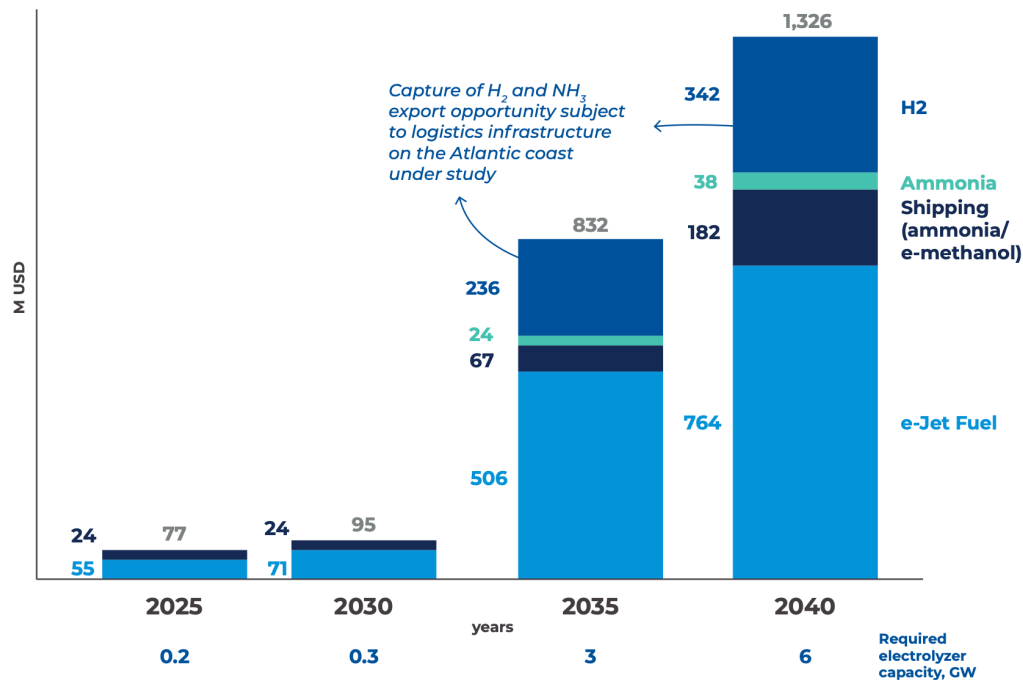


Figure 2: Exportation turnover (MIEM, 2022)

## 1.2 CO<sub>2</sub> capture technologies overview

There are three main pathways for capturing CO<sub>2</sub>. Firstly, in precombustion capture, the fuel is treated before combustion to prevent the CO<sub>2</sub> formation process (Garcia et al., 2022). However, this method is not suitable for already operational mills, especially pulp mills where there is limited flexibility to change the fuel.

The second method is Oxyfuel combustion, where the fuel is burned with nearly pure oxygen instead of air, allowing for CO<sub>2</sub> capture (Garcia et al., 2022). Nonetheless, this approach is not feasible for pulp mills, as all equipment, including recovery boilers and limekilns, is designed for air-combustion systems. Implementing pure oxygen combustion would require extensive redesigning of the recovery island in the pulp mill.

The last and most common CO<sub>2</sub> capture process is post-combustion capture. In this method, CO<sub>2</sub> is captured from the flue gases, and the module can be installed in already operational mills (Garcia et al., 2022). Within post-combustion technologies, there are various types, including absorption, adsorption, membranes, cryogenic distillation, and microbial conversion (algae) (Garcia et al., 2022). In the following sections, adsorption, membranes, and cryogenic distillation will be briefly explained. However, a separate chapter will be dedicated to absorption carbon capture methods due to their prevalence and wide usage.

When evaluating post-combustion carbon capture technologies, the two key parameters for technical comparison are capture efficiency and specific regeneration energy. The first is defined as the ratio between the mass flow or molar flow of CO<sub>2</sub> captured to the CO<sub>2</sub> in the flue gases. The second is the amount of energy needed for regeneration of the solvent per kilogram of CO<sub>2</sub> captured. These concepts will be addressed in detail in the following chapters.

### 1.2.1 Adsorption

In the adsorption process, CO<sub>2</sub> from flue gases is adsorbed by a solid material, involving a gas-solid interaction where the gas is deposited onto the adsorbent surface through physical or chemical bonding (Sadeghalvad et al., 2022, p. 3). The adsorption capacity relies on the physical and chemical properties of both the gas and solid phases. Regarding regeneration, the driving force can be temperature, pressure, or vacuum swing, allowing for the use of steam or electricity as energy sources (Sadeghalvad et al., 2022, p. 3).

Compared to other technologies, adsorption shows potential for requiring less regeneration energy and offering high stability. However, the technology is not yet fully established and encounters some drawbacks (Garcia et al., 2022). The main drawbacks of the adsorption process are heavily dependent on the adsorbent used. However, in general, the development of new adsorbents aims to increase capturing efficiency and selectivity, areas where liquid absorption can make a difference (Garcia et al., 2022).

### 1.2.2 Membranes

The working principle of membrane carbon capture (CC) involves the absorption of CO<sub>2</sub> by a solid membrane that is transparent to other flue gas components. In this regard, it offers several advantages over other technologies: it does not require high temperatures for regeneration, there are no waste streams, and it boasts high capture efficiency (Garcia et al., 2022).

However, membranes also have notable disadvantages. These include degradation at higher temperatures, reduction in permeability due to fouling, and sensitivity to moisture and acid present in the flue gases (Garcia et al., 2022). Additionally, while membranes are suitable for high concentrations of CO<sub>2</sub> in flue gases (>20%), they may face challenges when dealing with smaller concentrations (Garcia et al., 2022).

### 1.2.3 Cryogenic separation

In cryogenic separation, the flue gas is cooled to a temperature slightly above the solidification point of CO<sub>2</sub> frost. Subsequently, the gas is further cooled through expansion, causing the CO<sub>2</sub> to precipitate in the form of a liquid/solid slurry (approximately -100°C). The purified flue gas is then warmed and released into the atmosphere, while the slurry fraction undergoes solid/liquid separation to increase the CO<sub>2</sub> concentration from 10% to 90%. The solid CO<sub>2</sub> is heated to its melting point and then pumped in liquid form to the desired pressure and temperature conditions (Hoeger et al., 2021).

One significant advantage is that the CO<sub>2</sub> exits the process in liquid form, potentially saving energy and costs in downstream processes. Additionally, cryogenic separation can capture other pollutants with higher pressure than CO<sub>2</sub>, including SO<sub>x</sub> and NO<sub>2</sub> (Hoeger et al., 2021). However, drawbacks include challenges in managing frost formation, which can reduce the rate of heat exchange. Moreover, cryogenic separation is primarily used in precombustion applications where CO<sub>2</sub> concentrations are higher and is less common in cases where CO<sub>2</sub> is diluted (Garcia et al., 2022). Notably, Airliquide offers a cryogenic CC product that requires CO<sub>2</sub> concentrations higher than 15% (Barlow et al., 2023).

## 2 Main absorption CO<sub>2</sub> process

As mentioned earlier, only post-combustion processes are relevant for application in existing pulp mills. Among multiple technologies, the absorption process based on liquid solutions has been by far the most used and developed (Regufe et al., 2021). This section provides an overview of current

absorption technologies and evaluates each concept in terms of Technology Readiness Level (TRL), scalability, established projects, and general pros and cons.

Various absorbents are utilized in the chemical absorption process, including amine-based, carbonate-based, polymeric solvents, poly-ionic liquid, and enzyme solvents, among others (Peu et al., 2023). Moreover, multiple blends of solvents are under study to obtain the benefits of each type (Peu et al., 2023). Due to the extensive list of solvents used, this research will focus only on the most commonly used ones, namely amine-based and carbonate-based solvents (Peu et al., 2023). Additionally, an enzyme-based solvent is being studied in Swedish under the framework of the ACCSESS project (ACCSESS, 2022). Some insights into enzymatic solvents will also be provided in this chapter, as they are currently being tested in pulp mills.

## 2.1 Amine-based solvents

Amine-based solvents include primary, secondary, and tertiary amines, classified based on the number of carbon atoms attached to the nitrogen atom (Jang, 2016). Primary amines, such as monoethanolamine (MEA), are commonly used in solutions where they react with CO<sub>2</sub> in the flue gas stream to form carbamate species, facilitating CO<sub>2</sub> capture. However, challenges include amine degradation over time, resulting in reduced effectiveness and environmental concerns, as well as high energy consumption during solvent regeneration.

Secondary amines, despite facing challenges such as higher cost compared to primary amines, offer benefits such as enhanced thermal stability, potentially reducing degradation costs and byproduct emissions. Tertiary amines exhibit greater thermal stability compared to primary and secondary amines, potentially leading to longer operational lifetimes with reduced degradation (Peu et al., 2023).

Amines can be sterically hindered, meaning that the nitrogen atom is blocked by other groups, preventing larger molecules from reacting with the nitrogen atom in the amine. Consequently, carbamates formed by sterically hindered amines are less stable, requiring less energy for the regeneration process (Karlsson et al., 2021), and resulting in increased absorption capacity (Mokhatab et al., 2019). An example of a sterically hindered amine is DMP (2-amino-2-methyl-1-propanol).

### 2.1.1 MEA

In this process, the flue gas enters the absorption column, and the CO<sub>2</sub> is absorbed by the MEA solution. The clean flue gas exits the top of the absorber. The CO<sub>2</sub>-rich solution is pumped to the regeneration column (stripper), where it is first heated by the CO<sub>2</sub> lean solution in a heat exchanger (recuperator). The hot-rich solution then enters the stripper for desorption. Releasing CO<sub>2</sub> molecules from the MEA requires an energy input, provided by a reboiler at the bottom of the column. The CO<sub>2</sub> exits the top of the stripper, where water is removed in a condenser. The lean MEA exits the bottom of the reboiler and returns to the absorber to start the process again. The process diagram of the MEA process can be seen below in Figure 3.

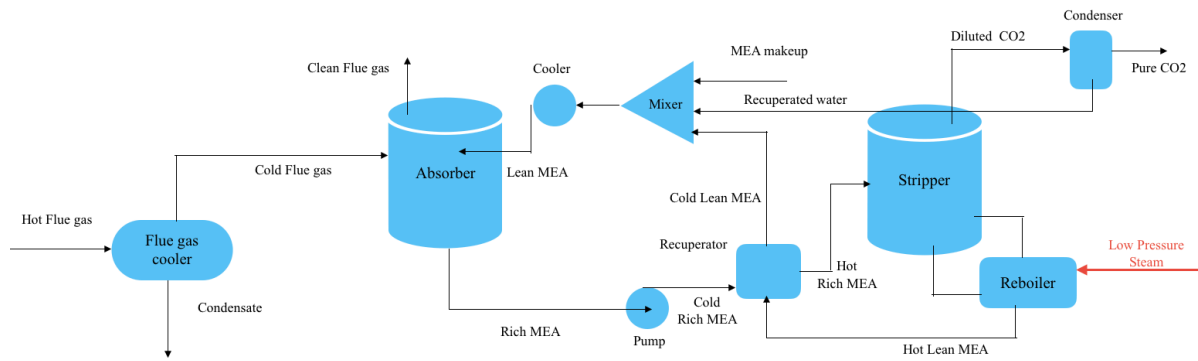


Figure 3: Typical MEA carbon capture

An important parameter when comparing energy requirements for the solvent regeneration is the reboiler duty. The total duty of the reboiler can be explained by the sum of three components as shown in Equation (1) (Warudkar et al., 2013)

$$q_{reb} = q_{sens} + q_{reac} + q_{stripping} \quad (1)$$

Where:

$q_{reb}$ : Is the total heat in the reboiler

$q_{sens}$ : Is the sensible heat until the reaction temperature

$q_{reac}$ : Is the energy of reaction

$q_{stripping}$ : Is the heat needed to produce the stripping steam

Warudkar et al. (2013) conducted a comparative analysis of various solvents, revealing that in the case of MEA, the principal contributor to higher reboiler duty is attributed to the stripping energy.

#### Technology readiness level, scalability, and established projects:

Traditional amine processes have a TRL of 9, indicating commercial availability and usage in various industries such as soda, fertilizers, natural gas plants, and cement plants (Kearns et al., 2021). This technology is well-established and proven at a large scale, with some projects capturing around 10 million tons per year (Hurtado, 2023).

#### Pros and Cons:

The amine-based process has an efficiency higher than 90% (Adu et al., 2020), with a rapid reaction velocity requiring a short residence time (Hu et al., 2016). However, drawbacks include the need for high thermal energy during regeneration, with a minimum of 120°C required in the reboiler (Aaron and Tsouris, 2005). Additionally, the absorbent experiences high degradation in oxidation environments, such as in post-combustion applications, necessitating continuous makeup of the MEA (Aaron and Tsouris, 2005). Finally, the amine-based process is associated with high corrosion rates in downstream installations (Hu et al., 2016).

#### 2.1.2 AMP/DMSO

As mentioned, the MEA process requires a significant amount of energy for regeneration, including sensible heat to increase the temperature to the reaction temperature, heat of the reaction for desorption, and heat generation for additional steam for stripping (Meldon, 2011). In the case

of MEA, the reaction temperature is typically above 120°C, leading to water evaporation and increased energy requirements (Karlsson et al., 2021).

An alternative to address the energy requirements for water evaporation is the use of a non-aqueous solution. AMP (2-amino-2-methyl-1-propanol) has been studied as an alternative. When combined with organic solvents like NMP (N-methyl-2-pyrrolidone), the absorption reaction produces a biphasic compound where CO<sub>2</sub> is captured in the form of AMP carbonates in solid form. Once the carbonates precipitate, they can be removed from the solution, reducing the amount of solution that needs regeneration and thus lowering energy requirements (Karlsson et al., 2021). However, NMP's toxic properties necessitate an alternative solvent such as DMSO (Dimethyl Sulfoxide) (Karlsson et al., 2021).

Using DMSO as a solvent, AMP carbonate can precipitate or remain in the liquid phase. Regeneration of AMP can occur at temperatures around (70-90)°C due to the steric hindrance composition of AMP (Karlsson et al., 2021).

#### Technology readiness level, scalability, and established projects:

Information regarding the TRL of the system is unavailable. However, the TRL of general sterically hindered amines, without specifying which amine is used, ranges from 6 to 9 (demonstration to commercial) depending on providers (Kearns et al., 2021). AMP/DMSO is being tested at a pilot plant scale (Tellgren, 2021) and is not yet commercially available.

#### Pros and Cons:

The main advantages include the lower regeneration temperature (<90°C), higher boiling point (reduced evaporation during regeneration), lower specific heat (reduced energy requirements in regeneration), and the possibility of adding a separation step to remove the solid form of AMP/CO<sub>2</sub>, thus reducing the amount of solvent entering the regenerator (Svensson, 2023). Currently, there are no clear negative aspects as extensive research is needed. This absorbent shows potential to overcome MEA drawbacks, but further experiments and research are required before commercial availability.

## 2.2 Carbonate-based solvent

Carbonate-based solvents are widely recognized in the industry for gas cleaning purposes. Among the most common are Sodium, Calcium, and Potassium carbonate.

Sodium carbonate, also known as soda ash, is a chemical compound extensively utilized in various industries for absorbing carbon dioxide (CO<sub>2</sub>). It is highly regarded for its efficiency and cost-effectiveness in removing CO<sub>2</sub> from gas streams. The process involves CO<sub>2</sub> reacting with sodium carbonate to produce sodium bicarbonate and carbonate ions. Sodium carbonate can be chemically regenerated through the addition of acid or thermally regenerated with energy input (Peu et al., 2023).

Calcium carbonate is also a used CO<sub>2</sub> absorbent due to its affordability, safety, availability, and eco-friendliness. Additionally, it shows a high capacity for absorbing CO<sub>2</sub>. The absorption process, known as carbonation, involves CO<sub>2</sub> being absorbed by calcium carbonate. However, a primary challenge in utilizing calcium carbonate as a CO<sub>2</sub> absorbent is its relatively low reactivity and solubility compared to some other absorbents, needing a longer residence time and higher CO<sub>2</sub> concentrations for efficient absorption (Peu et al., 2023).

Among carbonate-based solvents, Potassium Carbonate (K<sub>2</sub>CO<sub>3</sub>) emerges as a promising CO<sub>2</sub> absorbent due to several favorable characteristics. These include its cost-effectiveness, low

degradation rate, minimal toxicity, solubility in carbonate/bicarbonate solutions, and lower energy consumption during usage (Peu et al., 2023).

### 2.2.1 HPC (Hot Potassium Carbonate)

In the case of HPC, the sorbent used is potassium carbonate ( $K_2CO_3$ ). The working principle is similar to MEA, where  $CO_2$  is absorbed by potassium carbonate and then released in the desorber, where potassium carbonate is regenerated. However, a key difference from the MEA process is that HPC operates as a pressure swing process. Typically, the absorber operates at 15 bar, while the stripper operates at atmospheric pressure (Salvador Palacios, 2023). Consequently, electricity is required to run the compressor to achieve the pressure difference between the absorber and the desorber. Additionally, thermal energy is needed due to the endothermic reactions in the desorber, although the requirement is much lower than with MEA, usually with hot water being sufficient (Gustafsson et al., 2021).

#### Technology readiness level, scalability and established projects:

The TRL of HPC is reported as 9 by Kearns et al. (2021), while Fagerström et al. (2021) suggests a TRL of 7. The utilization of potassium carbonate ( $K_2CO_3$ ) for gas cleaning originated in the 1960s for coal gasification plants and has since been widely used, known as the "Banfield" process (Gustafsson et al., 2021). However, in synthetic gas cleaning, where the gas is already pressurized, compression is unnecessary. HPC is a relatively new technology for post-combustion applications, particularly where the partial pressure of  $CO_2$  is very low (Gustafsson et al., 2021).

HPC is being utilized in certain industries, such as refinery gas in Stockholm (Levihn et al., 2019). It is also part of the portfolio of gas-cleaning companies like Honeywell (Barlow et al., 2023). Furthermore, the Stockholm Exergi KVV8 project, currently in the pre-engineering phase, involves capturing  $CO_2$  from a biomass-based combined heat and power plant (Levihn et al., 2019).

#### Pros and cons:

Compared to MEA, HPC requires less energy for regeneration (Ayittey et al., 2020) and can be regenerated by pressure difference, with electricity being the main requirement. Additionally, HPC is less corrosive than MEA (Hu et al., 2016), and it has lower degradation rates in post-combustion conditions (Gustafsson et al., 2021).

However, a significant drawback is the slow absorption reaction rate at post-combustion conditions, needing long residence time and thus larger absorption and regeneration columns, leading to higher capital costs (Navedkhan et al., 2022). To enhance the reaction velocity, various promoters have been studied, with the most common being monoethanolamine (MEA), diethanolamine (DEA), and piperazine (PZ) (Bergman, 2022).

Despite requiring less overall energy than MEA, the compression of gases at high volumetric rates can considerably increase electricity consumption and the size of the compressor. Therefore, the economic viability of the process is influenced by factors such as the price of steam or electricity and the availability or preference of the energy source.

### 2.3 Enzyme absorption carbon capture

The process flow diagram for enzyme absorption carbon capture is similar to that of any other absorption process, featuring one absorption column and one stripper column for regeneration.

In this method, the solvent utilized is the biological enzyme carbonic anhydrase, derived from the chemical reactions in human and animal respiration. Unlike compounds like MEA, biological

enzymes are non-harmful and non-corrosive. Moreover, the waste streams produced in the enzymatic process are environmentally friendly, avoiding the need for downstream treatment processes. An additional advantage of enzymes is that they do not require steam for regeneration. Waste heat sources at 80°C can be utilized as an energy source for enzyme and CO<sub>2</sub> stripping. Enzyme absorption processes can achieve the same efficiency as MEA processes, typically around 90% (Novozymes, 2023).

However, enzymes have drawbacks, notably their sensitivity to operational variations, particularly temperature fluctuations, as their temperature range is limited (Liao et al., 2022). Another challenge arises from the low solubility of CO<sub>2</sub> in liquid solutions, leading to lower conversion efficiencies (Liao et al., 2022).

#### Technology readiness level, scalability and established projects:

Enzyme carbon capture has a TRL of 8 (Barlow et al., 2023), indicating rapid development within the carbon capture industry. As of 2020, it had a TRL of 6 (Kearns et al., 2021), highlighting the pace of advancement in this field.

Regarding projects, enzyme carbon capture is used in a pilot plant of a Swedish pulp mill through the ACCSESS project, which involves collaboration between Saipem and Prospin. Saipem provides the enzymatic solvent, while Prospin offers an absorber design that requires smaller sizing, thus reducing capital investment (ACCSESS, 2022).

The development of enzyme carbon capture was initiated by CO<sub>2</sub> Solutions Inc. (CSI), and it was tested at a Canadian gas-fired power plant. This project successfully captured 10 tons per day of CO<sub>2</sub> with an efficiency of 90%. The capturing project operated for 2500 hours without solvent degradation or emission of harmful gases or liquids (Canada, 2015).

## 2.4 Summary of the chemical absorption technologies

Finally, Table 1 shows the summary of results with the information gathered from the previously mentioned sources. Some values of thermal energy requirement (in the regeneration) and TRL are in a range because more than one value has been found in the literature.

	TRL	Reference Projects / Suppliers	Main drawbacks	Thermal energy
MEA/H <sub>2</sub> O	9	AmineGuard™ & Amine Guard FS Process (Honeywell) OASE® blue technology for Post-Combustion CO <sub>2</sub> Capture (PCC) (Linde)* Advanced Solvent for Carbon Capture (ASCC) (Honeywell)*	High regeneration energy Amine degradation Toxic solvent	3-4 MJ/Kg CO <sub>2</sub>
AMD/DMSO	(6-9)	Petra Nova Carbon capture*** Mikawa Power Plant (Toshiba)	Not commercially available	NA
HPC	(7-9)**	Stockholm Exergi	Slow absorption reaction	1,5 Mj/Kg CO <sub>2</sub>
Enzymes	8	Saipem CO <sub>2</sub> Solutions ACCSESS Project	Enzymes instability Relative low conversión rate	2,4 Mj/Kg CO <sub>2</sub>

\*\*\* Are sterically hindered amines developed for each company. It is not exactly AMD/DMSO

\*\* Well proven technology but not in flue gas condition

\* Amine-based, no specification of the exactly amine composition

*Table 1: Summary of absorption technologies*

## 2.5 Motivation for choosing the amine-based carbon capture module

In (Hurtado, 2023) the Top 10 CC projects for 2023 are presented. These are large projects that became active in 2023 and have shared sufficient data.

Project	Technology Suppliers	Size (Million TPA)	Technology Type	Efficiency
Oil Sands CCUS Pathways to Net Zero	Honeywell UOP carbon capture technologies	10-12	Amine-based carbon dioxide capture	95%
The Wabash CO <sub>2</sub> Sequestration Project	Honeywell UOP carbon capture technologies	1.65	Ortloff CO <sub>2</sub> Fractionation unit, Polybed™ PSA unit	99%
The Go4Zero Project	Air Liquide, TotalEnergies	1.1	Oxyfuels combustion (Cryocap™ Oxy technology)	95%
Calpine Baytown Energy Center	Shell Catalysts & Technologies	1.5	Shell CANSOLV® CO <sub>2</sub> Capture System (Amine-based)	>90%
The Rocky Mountain Carbon Project	To be determined by October 2023	1 - 1.3	To be determined by October 2023 (Q4)	Not provided
Project Anthemis	Undisclosed	0.8	OxyCal concept: Oxyfuel and Amine capture technology	97%
CalCC Lhoist Air Liquide Lime Plant Rety	Air Liquide	0.6	Cryocap™ FG (Flue Gas)	95%
Rohm Chemical Plant Decarbonization Project	Aker Carbon Capture	0.5	Liquid amine solvent to absorb CO <sub>2</sub>	>90%
South Texas Direct Air Capture Hub (DAC 1)	Carbon Engineering Ltd (bought by OXY in August 2023)	0.5 - 1	DAC Potassium hydroxide solution/calcium carbonation	99%
Removr Large-Scale Plant DAC Project	Removr	0.002 - 0.1	Zeolite DAC technology	Not provided

Table 2: Carbon Capture Main Projects from Hurtado., (2023)

Among these large-scale projects, a significant majority—4 out of 5 post-combustion capturing methods—are based on amine-based processes. The remaining methods include one cryogenic capturing, two oxyfuel combustion, and two direct air capture projects. Despite the acknowledged drawbacks of amine-based technologies, the prevailing market trend continues to favor them.

It's essential to note that when referring to amine-based technology, it doesn't necessarily imply MEA. Many ongoing projects are based on specific amines developed by private companies, with exclusive formulations aiming to reduce regeneration energy. However, MEA can serve as a benchmarking solvent, providing sufficient information and studies for valuable comparisons.

It is widely understood that amine-based solvents developed by private companies require less regeneration energy than MEA. Thus, modeling with MEA provides conservative estimates, as any other amine-based solvent would potentially require less energy. Additionally, the process integration analysis for MEA is typically more difficult due to higher temperature levels.

Regarding Hot Potassium Carbonate (HPC), it is often not considered alone as a solvent due to the necessity of larger columns. Blending with promoters is common practice, but the modeling tools for such blends are beyond the scope of this thesis. Moreover, energy calculations conducted by (Nilsson, 2023) comparing HPC and MEA in a pulp mill indicate that HPC requires more total energy when accounting for compressor work.

After weighing the arguments presented in the previous sections, the chosen technology for modeling in this thesis is MEA carbon capture. This choice does not imply that the mill should adopt this technology in the future. Rather, it serves as a baseline for comparing requirements against other technologies. Furthermore, considering the rapid expansion of the CC industry, technologies are transitioning from pilot plants to commercial availability fast. If the enzymatic pilot plant installed in Skutskär's pulp mill proves successful, it has the potential to become the first carbon capture system for a pulp mill.

### 3 Pulp mill basic operation description

The raw materials used in pulp production vary depending on the location of the mill, leading to minor adjustments in the process due to differences in tree composition. In Northern Europe, softwood trees like Fir, Pine, and Spruce are utilized, resulting in long fiber pulp due to the longer fibers present in softwood (Numera Analytics, 2023). Conversely, pulp mills in South America and warmer regions use hardwood such as Eucalyptus and Acacia, producing short-fiber pulp (Numera Analytics, 2023) The process is illustrated in Figure 4, this process representation is a simplified diagram of Mdp.

Upon arrival, wood is directly fed from trucks into the chipping machine, where it is cut into chips of specific dimensions (25 mm long, 25 mm wide, and 4 mm thick) to ensure proper liquor impregnation and subsequent processing (Quinde, 2020). Chips that deviate from this size are separated and incinerated in a power boiler, along with waste wood that is too large or small for chipping. In some cases, a debarking process precedes chipping, with the bark also incinerated in the Power Boiler (PB) (Quinde, 2020). However, there is no debarking process in Mdp.

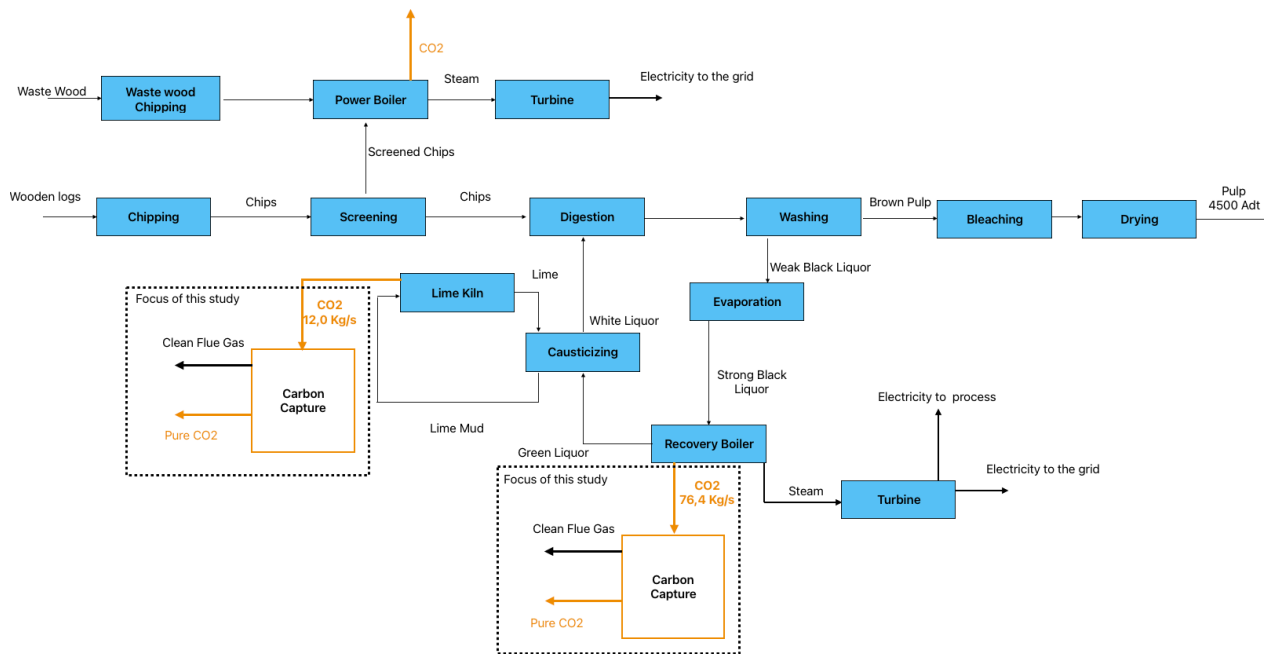


Figure 4: Simplified pulp mill process diagram with carbon capture (Robano and Nuorimaa, 2023)

Following chipping, the chips undergo cooking in the digester, using white liquor ( $\text{NaOH} + \text{Na}_2\text{S}$ ) at approximately  $150^\circ\text{C}$  to separate lignin from fibers (Tappi, 2019). The resulting mixture of fibers, lignin, and chemicals undergoes a washing process to purify the fibers from lignin and chemicals. Purified fibers then proceed through the pulp line for bleaching and drying until reaching the desired white pulp stage (Tappi, 2019). The residual mixture of chemicals and lignin known as Black Liquor (BL), contains essential cooking chemicals, necessitating recovery ( $\text{NaOH} + \text{Na}_2\text{S}$ ). Before entering the Recovery Boiler (RB), where these chemicals are recuperated, BL passes through an evaporator to increase dry solid content (approximately from 20% to 70%) (Tappi, 2019).

After concentration, BL is burned in the RB to recover chemicals, generating high-pressure steam (HPS) and passing through various stages such as air superheater, evaporator, economizer, and air preheater (Tappi, 2019). Smelt, comprising inorganic components of BL ( $\text{Na}_2\text{SO}_3$ ,  $\text{Na}_2\text{S}$ ,  $\text{NaCl}$ , etc.), is collected at the furnace bottom, containing recoverable chemicals that are dissolved in water in the dissolving tank to form green liquor.

Green liquor is then transferred to the causticizing plant, which is mixed with lime to form white liquor and then returned to the digester. Notably, lime is produced internally through the lime kiln process by the calcination of the limestone ( $\text{CaCO}_3 \rightarrow \text{CaO} + \text{CO}_2$ ).

Figure 4 shows the emissions for a daily pulp production of 4500 air-dry tonnes (Adt). The CO<sub>2</sub> emissions mainly come from two sources: the RB due to the combustion of BL, and the LK due to combustion in the burner and the calcination reaction. Currently, most lime kilns use fossil fuels, relying on fuel oil or natural gas. At MdP, the lime kiln burner uses heavy fuel oil. It should be noted that there is a third CO<sub>2</sub> source, the power boiler (PB). However, due to its relatively small CO<sub>2</sub> emissions compared to the LK and RB, the PB will not be considered in this study.

### 3.1 Steam cycle in a stand-alone mill

Stand-alone mills are mills that produce their own steam, electricity, and condensate internally. Their only interaction with the grid is for selling or buying electricity. Most of the time, the mill injects electricity into the grid. However, due to unexpected situations, it may occasionally need to purchase electricity for short periods, though this is not a typical operation.

Figure 5 presents a simplified representation of the steam and condensate circuit of MdP. The high-pressure steam (HPS) is produced in the RB and PB, the generation pressure is around 94,8 bar(g), and part of that steam is directly extracted from the superheaters and used for soot blowing after a pressure reduction valve. The soot-blowing pressure is around 20 bar(g).

Downstream the boilers, there are two turbines, one back pressure (TG1), and a condensation turbine (TG2). Both of them have medium pressure (MP), 13 bar(g), and low pressure (LP), 4,2 bar(g) extractions that are used in the process. The excess of steam that is not used in the process is expanded completely until the condenser pressure of -0,9 bar(g). The cold fluid for the condenser is water from the cooling tower (25-30°C).

In normal operation, the excess of steam that goes to the condenser is around 60 kg/s. In that operation point, the mill uses approximately 90 MW of electricity and injects 87MW into the grid. It should be noted that Figure 5 represents a simplified model, in reality, there are bypasses to the turbines, reduction valves, auxiliary tanks for MPS and LPS, makeup of treated water, etc.

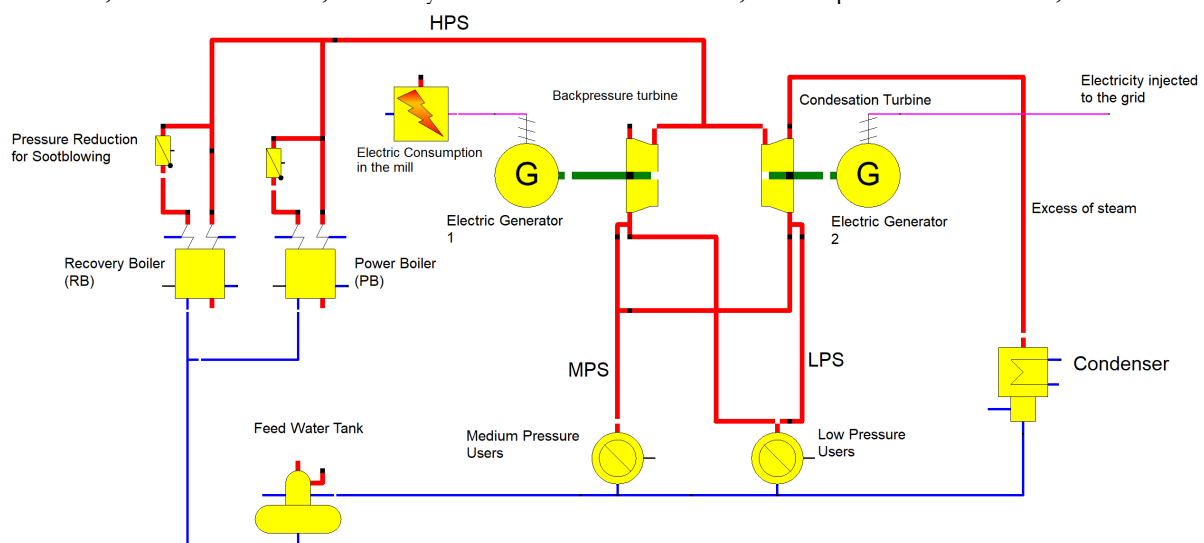


Figure 5: Steam and condensate simplified flowsheet

### 3.2 Warm and Hot water production

In stand-alone mills, warm (45°C) and hot (80°C) water are generally produced. Since the mill is not connected to any district heating network, this water is used within the process. However, any excess water is cooled in the cooling towers or discharged into the effluent plant. Despite their low temperatures, these sources of waste energy have the potential to serve as heat sources for other processes, thereby partially reducing steam consumption. Furthermore, they can potentially be utilized as heat sources in a heat pump configuration.

Warm water (WW) is produced for almost all subprocesses, with a surplus of approximately 3000 l/s at around 45°C. The hot water (HW) flow considered in this thesis comes from the scrubber of the vent gas from the dissolving tank, with an estimated flow of 120 l/s at a temperature of 85°C.

## 4 Literature review

The literature review will be specific to MEA carbon capture (CC) in pulp mills from a modeling and process integration approach. Studies purely economic have not been considered.

Arango Munoz (2020) has modeled an MEA carbon capture process for a pulp mill. In this thesis, the CC is modeled and validated following the procedure of Madeddu (2018). During the validation not only the kinetic parameters are changed, but also Henry's constants. However, the set of parameters that gives the best correlations is the ones of Aspen 2014 model (Li B.H. et al., 2014). In the end, the pressure of the stripper and the discharge pressure of the CO<sub>2</sub> compression station are changed to reduce the reboiler duty. When it comes to process integration, it is done only by studying the carbon capture process itself and not analyzing the waste streams of the rest of the mill. The sensitivity analysis is only done for the stripper pressure and the discharge compression pressure, without considering other parameters such as stripper inlet temperature and capturing efficiency.

In Hedström, (2014) different technologies of CC have been modeled in Aspen Plus. In the model are used 20 stages (axial discretization points). Further in this thesis, it will be shown that there is a minimum of stages number to be calculated, otherwise, the model will deviate from the experimental results. This problem could be solved if a methodology such as used in (Madeddu, 2018) would be used. From an integration point of view, the process integration has been only analyzed within the MEA process. There are no pinch analysis or steam-saving options for the other processes of the pulp mill.

With more focus on process integration, Frida Nilsson has analyzed three different CC technologies implementation for pulp mills (Nilsson, 2023). The thesis uses the previous study from (Pedersén and Larsson, 2017) where the waste heat sources and steam-saving options for the study case have been already identified. The process goes from the utilization of heat pumps to the valorization of the flue gases. From a modeling perspective, there is no modeling in Aspen Plus, the mass and energy balances are done by calculation. Furthermore, many values needed for the balances have been taken from other Aspen models of other researchers.

Surbamani (2022) has done a techno-economic analysis of two CC technologies (MEA and Chilled Ammonia). The modeling has been done using Aspen Hysis and validated against pilot plant data. However, the assumption of thermodynamic equilibrium and not considering MEA degradation temperature deviates the results from reality. Furthermore, in the validation, only the final results are compared (capture efficiency and reboiler duty), not the liquid temperature profile of the columns. From an integration perspective, there is no analysis of the heat exchanger network or

heat pump implementation. It is only calculated how much steam is needed and how much is available. The focus is more on the economic values, steam price, electricity price, interest rate, and investment in the CC.

In (Skoglund et al., 2023) the focus was on process integration. Utilization of pinch analysis and the development of the grand composed curve were performed to identify the process integration opportunities. A similar study has been done (Pedersén and Larsson, 2017) using the same procedure, but in this case, the opportunities of reducing low-pressure steam have been dimensioned indicating the impact on the process. However, in the first case, the modeling was done with all the default values, without any validation case, or further explanation about the model. Only the main results of the model were used.

Parkhi et al., (2023) have modeled MEA CC for two different pulp mills in the US. The novelty of the paper is that they integrate the Aspen model with a tool that optimizes the main streams to obtain the minimum capture cost. However, in this paper, there is no validation of the model or explanation of column profiles. In terms of integration, there is no analysis of waste heat valorization. Only the utilization of excess steam has been done with the focus on associated costs.

In addition to these studies, there are multiple Aspen Plus modeling studies on MEA, but none specifically for pulp mills ((Madeddu, 2018), (Li B.H. et al., 2014), (Wang et al., 2023)). These studies will be a guide in the modeling and validation sections, as the simulation procedure remains independent of the flue gas source.

As can be seen from all these papers, there is no research with a real study case where MEA CC modeling and process integration have been studied for the same case. On one hand, the papers with a focus on process integration, assume energy values and results from previous MEA models. The ones that analyze the energy efficiency of the pulp mill, just mention that the steam saving can be used for carbon capture, without doing the calculations. On the other hand, the papers with a focus on modeling, only do a superficial process integration, without studying deeper integration options within the pulp mill.

Having mentioned the literature gap, this thesis will focus on both modeling and real process integration study. The advantage of including both analyses in the same study case is that the behavior of the operational parameters of the MEA CC, such as stripper pressure or rich temperature, can be analyzed and can be seen as an extra variable for the process integration. Additionally, the model can be used as a way of predicting the outcome of different operation points when the CC has been implemented. Related to the process integration, analyzing all the streams of the mill and doing a pinch analysis is a thesis itself. In this case, some specific steam-saving options will be analyzed for the M<sub>d</sub>P study case. These steam-saving opportunities are the result of an extensive study done in (Pedersén and Larsson, 2017) which several pinch violations have been found and potential solutions have been proposed.

## 5 MEA CC in Aspen Plus: Modeling, calibration, and validation.

Before modeling the real study case, the model needs to be calibrated and validated against experimental data found in the literature. In this section, the main modeling parameters and decisions will be explained. Secondly, the kinetic parameters will be selected, and finally, the complete model will be validated.

The modeling of the complete MEA process will be divided into three phases: first, the model of the absorption column; second, the model of the stripper; and finally, closing the cycle as shown

in Figure 5 by modeling the heat exchanger, pump, and condenser. In the next section, the modeling of the columns will be explained.

For the modeling, calibration validation and finally understanding of the governance equation the final PhD thesis of Claudio Madeddu, (2018) has been utilized as a guide and has provided relevant knowledge about chemical reactors such as the absorber and stripper.

### 5.1 Columns modeling: Mass and energy balances

An important parameter that will be mentioned from the beginning is the number of stages. This is an axial discretization of the column used in the simulation where the chemical reactions, energy, and mass transfer occur. Aspen solves the discrete energy and mass balances for each stage.

In the absorber, the gaseous CO<sub>2</sub> is transformed into a liquid and then reacts with the MEA. The flue gas is injected from the bottom of the column and travels upwards, exchanging mass and energy and reacting at each stage. In the stripper, the CO<sub>2</sub> detaches from the MEA and is transformed into a gaseous phase, leaving the stripper as a gas. Figure 6 represents the stage number as the axial discretization of the absorber, in this case, “j” represents the stage number.

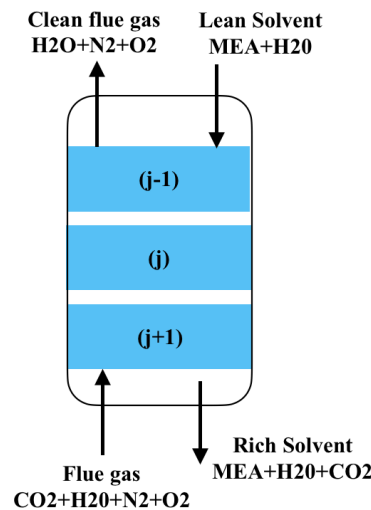


Figure 6: Stage number representation for the absorber

It is highlighted that the reactions occur in the liquid phase; there are no gas-phase reactions. The phenomena involved in the absorption and stripping processes are energy and mass transfer and chemical reactions. There are two model options in Aspen: Equilibrium and Rate-Based model. The first one assumes liquid and gas phases are in thermodynamic equilibrium at every stage. This is an ideal case when infinite residence time and a large exchange area are considered (Ramesh et al., 2007). In the equilibrium model there is no exchange of energy and mass between the liquid and gas phases.

As shown in Figure 7, there are mass and energy exchanges between the phases (through the interphase) and with the neighboring stages. Furthermore, as the reaction is in the liquid phase, there are sources of energy and mass in the liquid. The only mass and energy flow is from the previous and next stages as well as from the reaction.

For this thesis, the "rate-based model" will be employed to achieve more realistic results. The rate-based model assumes equilibrium only at the interface between the liquid and gas phases, with heat and mass transfer treated differently in the bulk phases (Madeddu, 2018). Figure 7 illustrates the

exchange of mass and energy in the different zones of the stage. The interphase will be modeled using the "two-film theory" of Lewis & Whitman. As it is treated differently from the bulk zones, the energy and mass balances will be present separately.

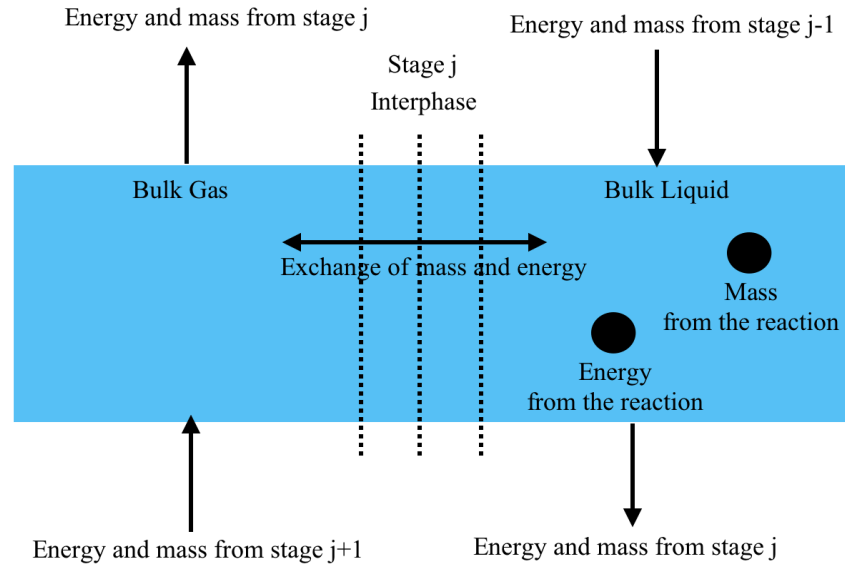


Figure 7: Stage representation adapted from Madeddu., (2018)

### 5.1.1 Mass and energy balance: Bulk liquid and gaseous phases

Aspen works by solving the discrete conservation equations of mass and energy for each stage in the axial direction.

Material balance in the bulk liquid phase: In can be seen the reaction term, since the reaction is the liquid phase.

$$\frac{dM_{i,j}^L}{dt} = L_{j-1}x_{i,j-1} - L_jx_{i,j} + \dot{N}_{i,j}^L + \dot{N}_{i,j}^R \quad (2)$$

Where:

L: As a superscript represents the liquid phase

i: Indicates the chemical component i

j: Indicates de stage number

$M_{i,j}^L$ : Are the liquid mols of the component i in the stage j [kmol]

$L_j$ : Liquid molar flow  $\left[\frac{\text{kmol}}{\text{s}}\right]$

$x_i$ : Molar fraction of substance i [mol frac]

$\dot{N}_i^L$ : Interphase liquid molar flow rate  $\left[\frac{\text{kmol}}{\text{s}}\right]$

$\dot{N}_i^R$ : Molar reaction rate  $\left[\frac{\text{kmol}}{\text{s}}\right]$

Material balance in the bulk gas phase: Note the absence of the reaction term.

$$\frac{dM_{i,j}^G}{dt} = G_{j+1}y_{i,j+1} - G_jy_{i,j} - \dot{N}_{i,j}^G \quad (3)$$

Where:

G: As a superscript represents the gaseous phase

$M_{i,j}^G$ : Are the gaseous mols of the component i in the stage j [kmol]

$G_j$ : Gaseous molar flow  $\left[\frac{\text{kmol}}{\text{s}}\right]$

$y_i$ : Molar fraction of substance i [mol frac]

$\dot{N}_i^G$ : Interphase gaseous molar flow rate  $\left[\frac{\text{kmol}}{\text{s}}\right]$

Energy balance in the bulk liquid phase

$$\frac{dU_j^L}{dt} = L_{j-1}h_{i,j-1}^L - L_jh_{i,j}^L + \dot{E}_j^L + \dot{Q}_j^R \quad (4)$$

Where:

L: As a superscript represents the liquid phase

i: Indicates the chemical component i

j: Indicates the stage number

$U_j^L$ : Energy in the stage j [kJ]

L: Liquid molar flow  $\left[\frac{\text{kmol}}{\text{s}}\right]$

$h_i^L$ : Specific enthalpy of substance i  $\left[\frac{\text{kJ}}{\text{Kg}}\right]$

$\dot{E}_j^L$ : Interphase energy flow  $\left[\frac{\text{kJ}}{\text{s}}\right]$

$\dot{Q}_j^R$ : reaction energy flow rate  $\left[\frac{\text{kJ}}{\text{s}}\right]$

Energy balance in the bulk gaseous phase

$$\frac{dU_j^G}{dt} = G_{j+1}h_{i,j+1}^G - G_jh_{i,j}^G - \dot{E}_j^G \quad (5)$$

Where:

G: As a superscript represents the gaseous phase

$U_j^G$ : Energy in the stage j [kJ]

G: Gas molar flow  $\left[\frac{\text{kmol}}{\text{s}}\right]$

$h_i^G$ : Specific enthalpy of substance i  $\left[\frac{\text{kJ}}{\text{Kg}}\right]$

$\dot{E}_j^G$ : Interphase energy flow  $\left[\frac{\text{kJ}}{\text{s}}\right]$

In the next section, it will be shown how the interphase energy and mass balance are calculated.

### 5.1.1 Mass and energy balance: Interphase

Figure 8 is a simplified version of the interphase representation for the absorption process used in Madeddu., (2018). As can be seen, there are four regions, the two film (liquid and gas) and the two

bulk (liquid and gas). As it is represented for the absorber, the energy and mass flows are in the liquid direction. In the stripper would be the opposite direction. The following equations will show how Aspen calculates the interphase molar and energy flow used in the bulk energy and mass balance.

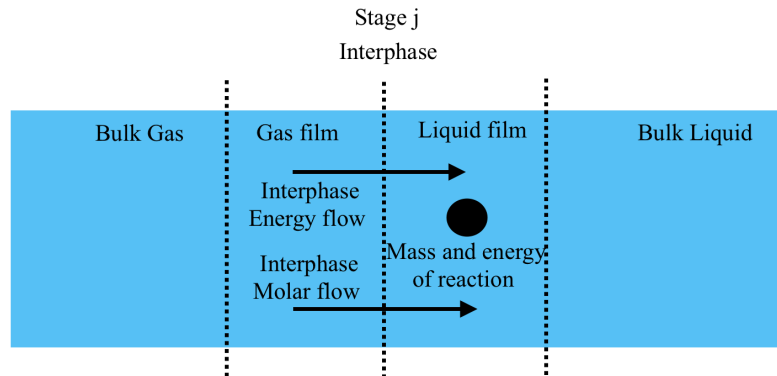


Figure 8: Interphase mass and energy exchange adapted from Madeddu., (2018)

Material balance in the liquid film:

$$\dot{N}_i^{\text{int}} = \dot{N}_i^{\text{L,R}} + \dot{N}_i^{\text{L}} \quad (6)$$

Where:

$\dot{N}_i^{\text{int}}$ : Interphase molar flow from gas phase  $\left[\frac{\text{Kmol}}{\text{s}}\right]$

$\dot{N}_i^{\text{L,R}}$ : Molar reaction rate at the interphase  $\left[\frac{\text{Kmol}}{\text{s}}\right]$

$\dot{N}_i^{\text{L}}$ : Interphase molar flux diluted into the liquid bulk  $\left[\frac{\text{Kmol}}{\text{s}}\right]$

Liquid molar flux in the interphase:

$$N_i^{\text{L}} = J_i^{\text{L}} + x_{i,\text{avg}} N_t^{\text{L}} \quad (7)$$

Where:

$N_i^{\text{L}}$ : Interphase molar flux diluted into the bulk  $\left[\frac{\text{Kmol}}{\text{m}^2\text{s}}\right]$

$J_i^{\text{L}}$ : Diffuse molar flux  $\left[\frac{\text{Kmol}}{\text{m}^2\text{s}}\right]$

$x_{i,\text{avg}}$ : Mean molar fraction of the component i in liquid phase

$N_t^{\text{L}}$ : Mixture molar flux  $\left[\frac{\text{Kmol}}{\text{m}^2\text{s}}\right]$

Material balance in the gas film;

$$\dot{N}_i^{\text{int}} = \dot{N}_i^{\text{G}} \quad (8)$$

Where:

$\dot{N}_i^{\text{int}}$ : Interphase molar flow from liquid phase  $\left[\frac{\text{Kmol}}{\text{s}}\right]$

$\dot{N}_i^{\text{G}}$ : Interphase molar flux diluted into the gas bulk  $\left[\frac{\text{Kmol}}{\text{s}}\right]$

Gas molar flux in the interphase:

$$N_i^G = J_i^G + y_{i,avg} N_t^G \quad (9)$$

Where:

$N_i^G$ : Interphase molar flux diluted into de bulk  $\left[\frac{\text{Kmol}}{\text{m}^2\text{s}}\right]$

$J_i^G$ : Diffuse molar flux  $\left[\frac{\text{Kmol}}{\text{m}^2\text{s}}\right]$

$y_{i,avg}$ : Mean molar fraction of the component i in gaseous phase

$N_t^G$ : Mixture molar flux  $\left[\frac{\text{Kmol}}{\text{m}^2\text{s}}\right]$

The  $J_i$  is calculated using the Maxwell-Stefan diffusion equations for multicomponent systems. These equations are not going to be presented in this thesis.

Energy balance in the Liquid film:

$$\dot{E}^{int} = \dot{Q}^{L,R} + \dot{E}^L \quad (10)$$

Where:

$\dot{E}^{int}$ : Interphase energy flow from gas phase  $\left[\frac{\text{Kmol}}{\text{s}}\right]$

$\dot{Q}^{L,R}$ : Energy reaction rate at the interphase  $\left[\frac{\text{Kmol}}{\text{s}}\right]$

$\dot{E}^L$ : Interphase energy flux to the liquid bulk  $\left[\frac{\text{Kmol}}{\text{s}}\right]$

Energy balance in the Gas film:

$$\dot{E}^{int} = \dot{E}^G \quad (11)$$

Where:

$\dot{E}^{int}$ : Interphase energy flow from gas liquid  $\left[\frac{\text{Kmol}}{\text{s}}\right]$

$\dot{E}^G$ : Interphase energy flux to the gas bulk  $\left[\frac{\text{Kmol}}{\text{s}}\right]$

And the interphase energy flux at gas and liquid phase is calculated by:

$$\dot{E}^L = q^L + \sum_i N_i^L (h_i + \lambda_i) \quad (12)$$

$$\dot{E}^G = q^G + \sum_i N_i^G (h_i + \lambda_i) \quad (13)$$

Where the first term ( $q$ ) is the conductive heat that can be calculated using Fourier's law and the second term is the sum of the enthalpy ( $h$ ) and the vaporization/condensation heat ( $\lambda$ ) for each component.

## 5.2 Columns modeling: Chemical reactions

There are 5 reactions involved in the MEA absorption and stripping process.

- 1)  $2\text{H}_2\text{O} \rightleftharpoons \text{H}_3\text{O}^+ + \text{OH}^-$  (Water ionization – Equilibrium)
- 2)  $\text{MEA}^+ + \text{H}_2\text{O} \rightleftharpoons \text{H}_3\text{O}^+ + \text{MEA}$  (MEA dissociation – Equilibrium)
- 3)  $\text{HCO}_3^- + \text{H}_2\text{O} \rightleftharpoons \text{H}_3\text{O}^+ + \text{CO}_3^{2-}$  (Bicarbonate ion dissociation – Equilibrium)
- 4)  $\text{CO}_2 + \text{MEA} + \text{H}_2\text{O} \rightleftharpoons \text{MEACOO}^- + \text{H}_3\text{O}^+$  (Carbamate formation – Kinetic)
- 5)  $\text{CO}_2 + \text{OH}^- \rightleftharpoons \text{HCO}_3^-$  (Bicarbonate ion formation – Kinetic)

By default, in Aspen the equilibrium constant for reactions 1),2), and 3) are calculated based on the change of standard Gibbs free energy (Technology, 2018) Equation (14).

$$K_{\text{eq}} = e^{\frac{-\Delta G^0}{RT}} \quad (14)$$

Where:

$K_{\text{eq}}$ : Equilibrium constant

$\Delta G^0$ : Variation of standard Gibbs free energy

T: Temperature

R: Universal gas constant

For the kinetic reactions, it is needed to define the rate of reaction. Equation (15) shows the expression for the reaction rate, where the concentration is on molarity basis

$$r = k e^{\frac{-ER}{T}} \prod_{i=1}^N (C_i)^{v_i} \quad (15)$$

Where:

r: Rate of reaction

k: Pre exponential factor

E: Activation energy

R: Universal gas constant

T: Temperature

$C_i$ : molarity component i

$v_i$ : Stoichiometric coefficient of component i

N: Total number of components

For each kinetic reaction it is needed to define k and E both values are obtained by literature review for the forward reactions and are by default in Aspen. The values from the reverse reaction are calculated using Equation (16)

$$k_r^a = \left( \frac{k_f^a}{k_{\text{eq}}^a} \right) \quad (16)$$

Where:

$k_f^a$ : Rate of constant forward reaction

$k_r^a$ : Rate of constant reverse reaction

$k_{\text{eq}}^a$ : Equilibrium constant

The kinetic data available in Aspen is summarized in Table 3. During the validation of the model, these values will be studied and compared with other researchers to achieve the best correlation with the experiments as possible.

Reaction	k (kmol/m <sup>3</sup> s)	E(cal/mol)	Reference
4 (Forward)	9,77E+10	9855,8	Hikita et al, (1977)
4 (Reverse)	3,23E+19	15655	Hikita et al, (1977)
5 (Forward)	4,32E+13	13249	Pinsent et al, (1956)
5 (Reverse)	2,38E+17	29451	Pinsent et al, (1956)

Table 3: Kinetic data available in Aspen Plus

### 5.3 Columns modeling: Profiles and transfer coefficients

In each stage of the column, it is expected to have different temperatures and CO<sub>2</sub> concentrations; consequently, each column will have a temperature and CO<sub>2</sub> profile in the axial direction. In the absorber, the highest CO<sub>2</sub> concentration in the gas phase is expected at the bottom of the column (flue gas injection), whereas in the stripper, the highest gas concentration of CO<sub>2</sub> will be found at the top.

The absorption reaction is exothermic, so the temperature is expected to change. As explained by Madeddu et al. (2019), the position of the temperature bulge is determined by the ratio of the liquid mass to the mass of gas (L/G) within the tower. When L/G is less than 5, the bulge is at the top part (near the inlet of MEA); when it is between 5 and 6, it is somewhere in the middle; when it is higher than 7, it is at the bottom of the column (near the outlet of MEA). This will be highlighted in the following validation cases.

As mentioned, the number of stages represents discretization points along the axial direction. The higher the number of stages, the more accurate the results, but this also increases the computational power required for each simulation. To determine the appropriate number of stages, the temperature profile of each column will be plotted for different discretization points. When these profiles coincide, it indicates that additional stages are unnecessary, following the approach proposed by Madeddu (2018).

During the modeling, other parameters need to be chosen and are based on empirical correlations available in Aspen. These correlations have been developed to model phenomena such as liquid holdup and energy and mass transfer coefficients. The decision between one correlation and another is highly influenced by the type of packing in the column. The options are random and structured packing. For this thesis, structured packing will be chosen, with the heat and mass transfer coefficients modeled by the empirical correlation of Onda et al. (1968) and the liquid holdup by Bravo et al. (1992).

### 5.4 Columns modeling: Geometrical and operational parameters

When modeling the columns, geometrical parameters such as diameter, height, and packing material are required as input. When modeling an existing pilot plant for validation, the geometrical and operational parameters will be provided. However, when a new column needs to be dimensioned, the dimensioning is done following a procedure that will be explained in the Results section.

For the operational parameters, such as pressure and temperature, the same approach applies. When modeling a pilot plant, this information is given. However, when dimensioning a new column, this information is taken from the literature.

The main operational parameters to be considered during the modeling of the columns have been taken from Madeddu et al., (2019). The reboiler duty is an input value that will be manipulated, the procedure is explained in the Results section.

- Modeling absorber: Operating pressure 1 bar
- Modeling stripper: Operating pressure 1.8 bar will be studied in Section “5.1.6 Sensitivity analysis for the RB: Variation of stripper operation pressure”

### 5.5 Modeling the external components

As shown in Figure 3, there are external components that need to be modeled to connect both columns. The modeling of these components does not require further explanation beyond the selection of operational temperature and pressure. Each component will be named as it is in Figure 3, the operational parameters for each component were taken from Madeddu et al. (2019)

- Flue gas cooler:
  - Pressure: 1,1 bar
  - Cold flue gas exit temperature: 40 °C
- Pump:
  - Rich MEA exit pressure: 1,8 bar
- Recuperator:
  - Type: Counter-current heat exchanger
  - No pressure losses
  - Hot rich MEA temperature: To be discussed in Section “5.1.5 Sensitivity analysis for the RB: Variation of stripper inlet temperature”
  - Minimum temperature difference: 10°C
- Condenser:
  - Pressure: 1 bar
  - Pure CO2 exit temperature: 40 °C
- Cooler:
  - Pressure: 1,1 bar
  - Lean MEA exit temperature: 40 °C

### 5.6 Kinetic parameters selection

For kinetic reaction 4), multiple kinetic factors have been found in the literature. Table 4 shows these values. However, studies where reaction 5 has been calibrated have not been found.

<b>k[kmol/m<sup>3</sup>s]</b>	<b>E[cal/mol]</b>	<b>Reference</b>	<b>Comment</b>
4,50E+11	10733,22	Kucka et al. (2003)	
1,17E+06	1797,1	Kvamsdal and Rochelle (2008)	
9,77E+10	9858,8	Hikita et al. (1977)	Aspen Default
6,83E+10	9855,8	Errico et al. (2016)	New proposed model

Table 4: Kinetic values for modelling reaction 4

To select the best representative kinetic data for reaction 4, results from different sets of kinetics are compared with experimental results using information from the pilot plant used by Tontiwachwuthikul et al., (1992). In this case, the experiment consisted of measuring the temperature and composition of an absorption column in 5 points. Table 5 summarizes the main parameters of the experiment.

Parameter	Value
Column height (m)	6,55
Column diameter (m)	0,1
Packing material	Ceramic Berl Saddles
<b>Flue gas</b>	
Flow (Kg/h)	15,16
Temperature (K)	288,15
Pressure (kPa)	103,15
CO2 (mol frac)	0,192
H2O (mol frac)	0,1
N2 (mol frac)	0,708
<b>Lean solvent</b>	
Flow (Kg/h)	75,46
Temperature (K)	292,15
Pressure (kPa)	103,15
MEA (mol frac)	0,0497
H2O (mol frac)	0,9503

Table 5: Pilot plant parameters from Tontiwachwuthikul et al., (1992).

As mentioned before, it is expected to have both a temperature and a CO<sub>2</sub> concentration profile in the column. The CO<sub>2</sub> gas concentration gradient is due to the gas becoming cleaner as it rises in the absorber column. In contrast, the liquid temperature profile is due to the absorption being an exothermic reaction, causing the temperature to change as the liquid falls.

Figures 9 and 10 show the liquid temperature and CO<sub>2</sub> vapor fraction for the different kinetic models listed in Table 4. It can be seen that the liquid temperature bulge is found near the bottom of the column, indicating an (L/G) ratio higher than 7

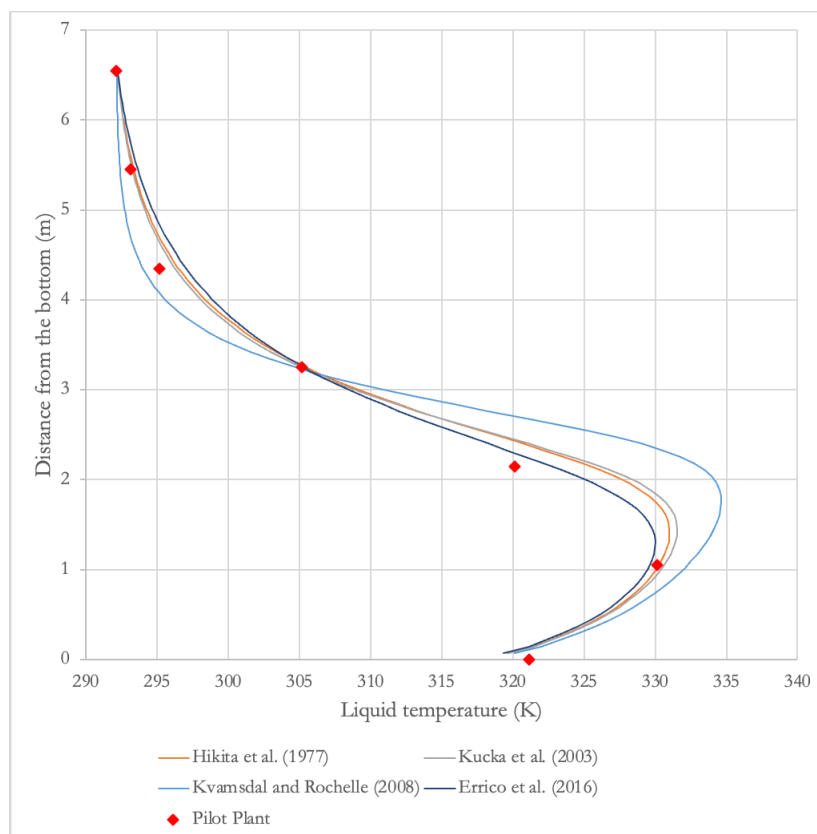


Figure 9: Liquid temperature in the absorber for different kinetic models

The model proposed by Kvamsdal and Rochelle (2008) is the one that has shown the most discrepancy, for the temperature and CO<sub>2</sub> vapor fraction. The models of Hikita et al. (1977) and Kucka et al. (2003) have very similar behavior and the lines are practically overlapping. The new model proposed by Errico et al. (2016) seems to perform better for some points and worse at other points for the liquid temperature. However, the CO<sub>2</sub> fraction seems to have some differences with the experiment at the top of the column (last 3 points). For that, the values of Hikita et al. (1977) are chosen for the rest of the simulations, since they lead to the best agreement both in liquid temperature and CO<sub>2</sub> fraction.

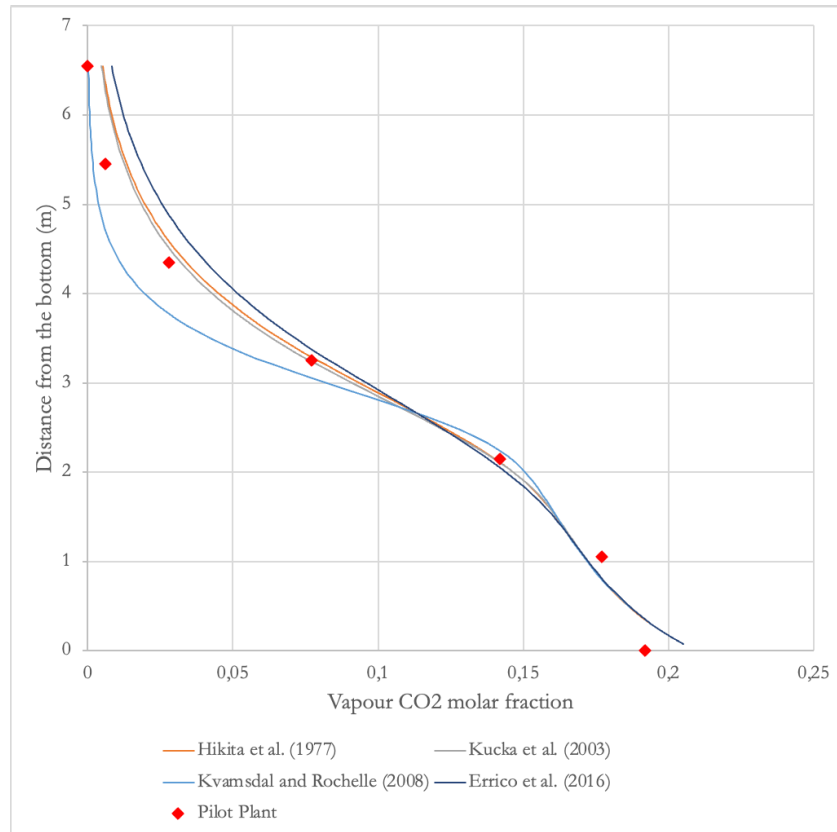


Figure 10: Vapour CO<sub>2</sub> fraction in the absorber for different kinetic models

The final results, considering Hikita et al. (1977) parameters are presented in Table 6.

	CO <sub>2</sub> capture efficiency	Rich MEA load (mol CO <sub>2</sub> / mol MEA)
Pilot Plant	100%	0,514
Model	98,00%	0,509

Table 6: Main results (model vs experiment from Tontivachwuthikul et al., (1992).)

### 5.7 Absorber validation

For the next validation case, the large-scale pilot plant from the CESAR project of the work from Razi et al., (2013) will be used. The pilot plant works with flue gases from a coal-fired power plant. Information of the CESAR pilot plant is shown in Table 7.

Parameter	Value
Column height (m)	17
Column diameter (m)	1,1
Packing material	Mellapack 2X
<b>Flue gas</b>	
Flow (Kg/s)	1,5
Temperature (K)	326,92
Pressure (kPa)	106,391
CO2 (mol frac)	0,12
H2O (mol frac)	0,12
N2 (mol frac)	0,76
<b>Lean solvent</b>	
Flow (Kg/s)	4,9
Temperature (K)	332,57
Pressure (kPa)	101,325
MEA (mol frac)	0,102
H2O (mol frac)	0,8717
CO2 (mol frac)	0,0263

Table 7: Experimental parameters from CESAR project from Razi et al., (2013)

Figure 11 shows the comparison of the temperature profiles for experimental and modeling cases. It should be noted that in this case only the kinetic parameters from Hikita et al., (1977) were used for the modeling.

Comparing the two temperature profiles of the validation cases from Figure 9 and Figure 11 it is illustrated how the temperature profiles are different. In the first case, the temperature bulge is at the bottom of the column, and in the CESAR pilot plant case (Figure 11), it is located at the top of the column. Indicating that in the CESAR pilot plant, the L/G ratio was less than 5.

It can be seen how the model captures the trend, with a difference of around 5 K at the top of the column. This validation case shows how the model can simulate the real behavior of the column, even with high flow rates.

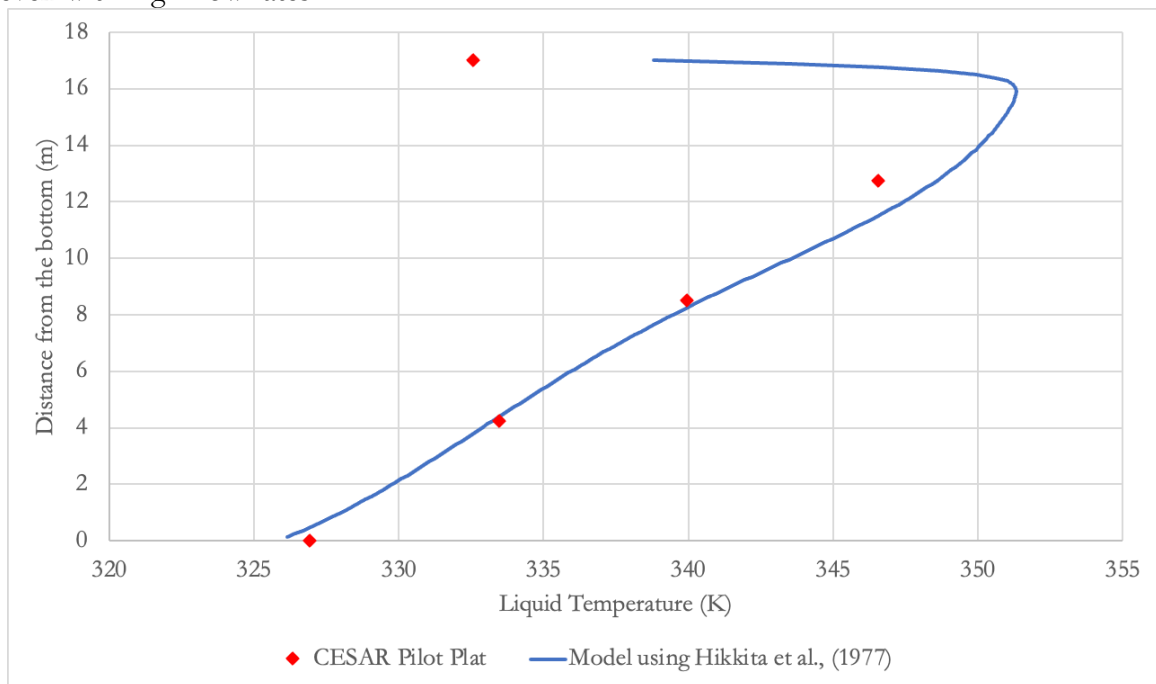


Figure 11: Temperature profile, model vs experiment CESAR

## 5.8 Stripper Validation

For the stripper validation, the experiments done by Tobiesen et al., (2008) in the SINTEF lab in Norway have been chosen. The experiment setup consisted of 5 measuring points, where the temperature has been measured. The reflux from the top condenser goes into the reboiler feed, and the lean regenerated solvent comes out from the reboiler. Table 8 shows the main experimental parameters used in the SINTEF Lab.

<b>Parameter</b>	<b>Value</b>
Column height (m)	3,89
Column diameter (m)	0,1
Packing material	Mellapack 250Y
<b>Rich Solvent</b>	
Flow (Kg/h)	253
Temperature (K)	389,81
Pressure (kPa)	106,391
CO2 (mol frac)	0,03484
H2O (mol frac)	0,8549
MEA (mol frac)	0,11026
<b>Operation conditions</b>	
Condenser pressure (kPa)	196,96
Condenser temperature (K)	288,15
Reboiler duty (kW)	11,6

*Table 8: SINTEF experiment parameters*

Results are presented in Figure 12. The difference between temperatures is around 1 K at the bottom of the column, showing a good agreement of the experiment and simulation. The model shows not only good agreement in the temperature profile but also in the final results. The molar flow from the condenser in the experiment was 0,11588 kmol/h and in the model 0,11577 kmol/h. Furthermore, the loading of the regenerated solvent in the model was 0,2033 mol CO<sub>2</sub>/mol MEA, and in the experiment 0,21852 mol CO<sub>2</sub>/mol MEA.

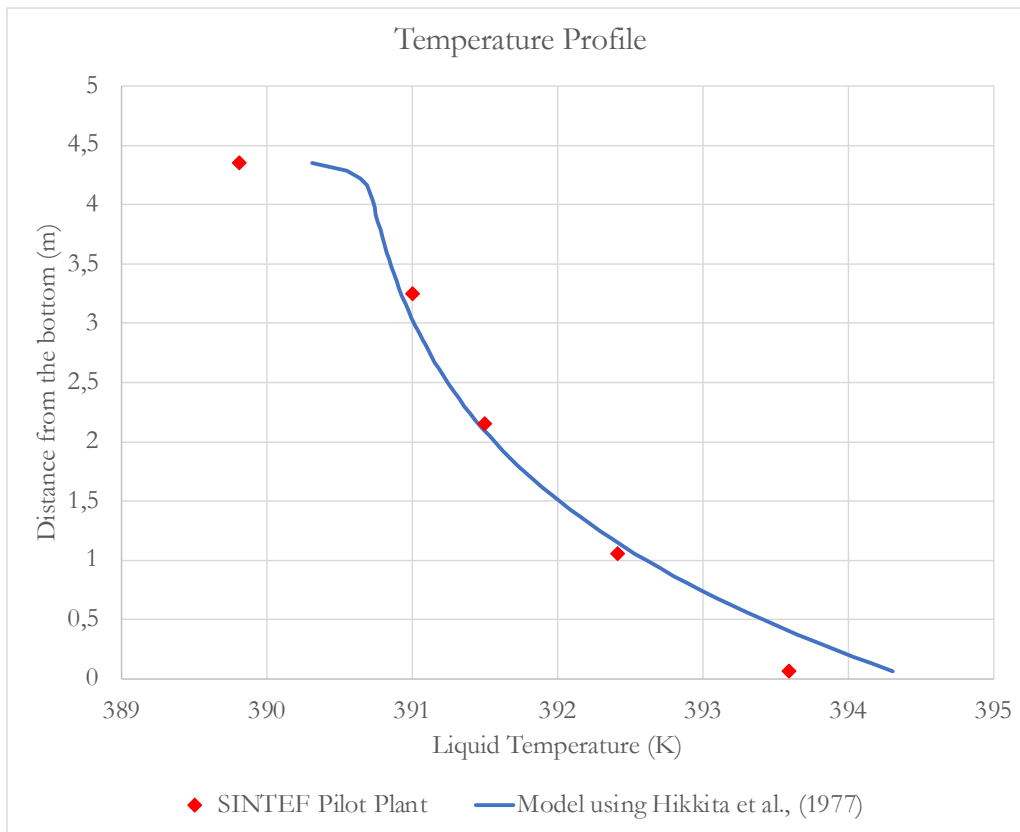


Figure 12: Temperature profile, model vs experiment SINTEF

Having validated the models. The next step is to simulate the MEA carbon capture for the case of MdP pulp mill. The main difference in the modeling procedure is that now, the dimensions of the columns are not known, and it is needed to do the dimensioning of the equipment. This will be done following the procedure from Madeddu, (2018) and it will be explained in the following section.

## 6 Results

It needs to be highlighted, that in this section the model explained before will be used. However, as the columns are not dimensioned yet, because it is a new installation. Hence, in this section the dimensioning procedure will be explained while showing the results.

The dimension of the MEA CC will be done for the Recovery Boiler (RB). After the main equipment has been dimensioned, a sensitivity analysis will be done in order to optimize the operational parameters. Finally, the model results will be shown for the Lime Kiln (LK) and the RB using the optimized operation parameters.

Based on the information received by MdP the flue gas from the RB and the LK are characterized by the parameters shown in Tables 9 and 10. This will be the main input for the further dimensioning of the absorber column.

It should be noted that in the case of RB and LK, there is no measure of CO<sub>2</sub>, N<sub>2</sub>, and H<sub>2</sub>O content in flue gases. Only O<sub>2</sub> content is measured. In the case of RB there is information about how much of each chemical component of the black liquor goes into the flue gases and an estimation of CO<sub>2</sub> content in the flue gases was given by the manager. With that information and knowing the O<sub>2</sub> content it was possible to calculate the other component fractions (CO<sub>2</sub>, H<sub>2</sub>O, and N<sub>2</sub>) by solving the combustion equation.

<b>Composition</b>	<b>molar (%)</b>
H2O	25
CO2	13
O2	3
N2	59
<b>Temperature</b>	140°C
<b>Mass flow rate</b>	370 Kg/s

*Table 9: Flue gas from MdP RB*

For LK flue gas composition, only by solving the combustion equation, it is not possible to know the Flue Gas (FG) composition. Because the calcination of CaCO<sub>3</sub> emits CO<sub>2</sub> and because the flue gases are used to dry the lime mud, consequently there is an amount of H<sub>2</sub>O and CO<sub>2</sub> content that does not come from the fuel. A typical level of CO<sub>2</sub> content was given and the O<sub>2</sub> was measured, with that information and compared with other researchers the composition of LK FG is given in Table 10.

<b>Composition</b>	<b>molar (%)</b>
H2O	34
CO2	18
O2	3
N2	45
<b>Temperature</b>	280°C
<b>Mass flow rate</b>	42 Kg/s

*Table 10: Flue gas from MdP LK*

For both cases, it should be mentioned that this is an approximation, there are NO<sub>x</sub>, CO, H<sub>2</sub>S, and Particulate Matter (PM) in the flue gases that have not been considered for the sake of simplicity and because the amount is so small that they did not have impact on the energy requirements for the CO<sub>2</sub> capture. Furthermore, for the stripper operation temperature used in this study, the content of these species was below the allowed values from MEA degradation (Zhou et al., 2012).

The dimensioning and sensitivity procedure will be done and explained only for the case of RB. For the LK the results will be just presented because the methodology has been the same for both cases.

## 6.1 Standard MEA CC for the RB

### 6.1.1 Absorber model for the RB

For the absorber dimensioning the MEA was considered with the following composition in Table 11. This is the composition of a commercial MEA solution at 30%. Some content of CO<sub>2</sub> was considered, assuming that is not possible a complete regeneration of the MEA in the stripper.

<b>Composition</b>	<b>Mass (%)</b>
H2O	65
CO2	5
MEA	30

*Table 11: Lean solvent composition*

Table 12 shows the standard design conditions for a CO2 absorber. As can be seen during the design process, the diameter, height and lean MEA mass flow rate need to be calculated.

Type	Packed
Packing material	Sulzer 250 Y
Working pressure	1 bar
CO2 capture efficiency	90% (molar)
Lean MEA temperature	40°C
Flue gas inlet temperature	40°C
Diameter	To be determined
Height	To be determined
Lean MEA mass flow rate	To be determined

*Table 12: Absorber modeling parameters*

As explained in the previous section, the operational parameters such as temperature and pressure were chosen based on the literature. The packed material chosen is structured packing, as explained earlier. The design condition of a capture efficiency of 90% was based on common design practices and will be discussed in detail in the sensitivity analysis.

As it was mentioned before first of all it is needed to choose the number of stages (axial discretization points) in Figure 13 can be seen the variation of the temperature profile for different stage numbers (N). It illustrates how there is practically no difference in the temperature profile for the 90 and 100 stages. Consequently, the number of stages chosen for the following model is 100 and there is no need to simulate again with 110 stages.

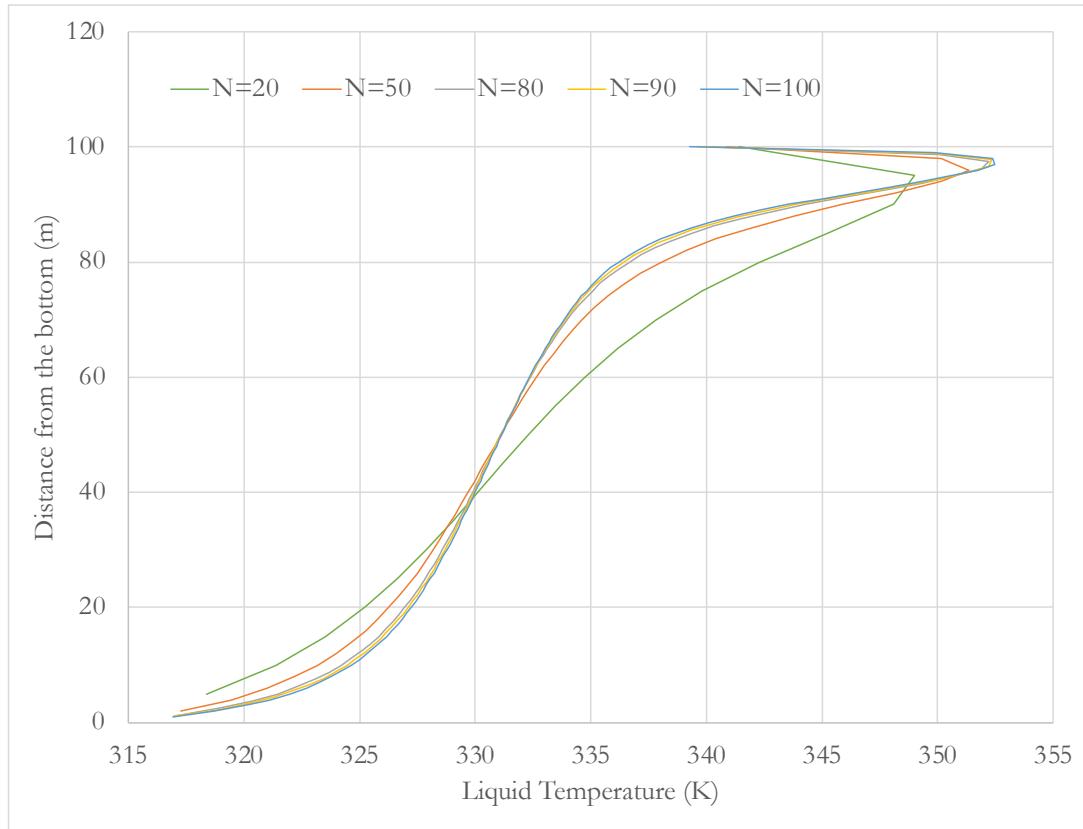


Figure 13: Variation of the stages number

To calculate the minimum diameter and minimum lean MEA flow rate, infinite height is considered. This means that the residence time will be high and a very small flow and diameter will be needed to absorb the desired CO<sub>2</sub>. With a fixed height (100 m) the diameter and lean MEA flow will be changed until the exhaust clean gas has a CO<sub>2</sub> molar flow of 10% of the inlet flow (90% of capture efficiency). The diameter is calculated automatically by Aspen based on the flooding velocity, that is the velocity where the steam flow is maximum. It is called the flooding velocity because is the velocity where the liquid can not fall and the stage starts flooding (Emerson, 2010).

In Table 13 it can be seen the results for each Lean MEA mass flow:

Lean MEA flow (Kg/s)	CO <sub>2</sub> out (kmol/s)	Diamter(m)	Capture efficiency
900	0,416	13,117	0,760
1000	0,277	13,534	0,840
1050	0,210	13,776	0,879
1060	0,197	13,829	0,886
1070	0,183	13,884	0,894
1080	0,170	13,941	0,902

Table 13: Main results absorber design

The first result from Table 13 is that the minimum diameter is 13,94 m. Based on Madeddu et al., (2019) the maximum recommended diameter cannot be bigger than 12 m. Consequently, it will be needed to install two absorbers in parallel, each of them with half of the flue gas mass flow. For

the rest of the project, only half of the flow will be modeled. At the end, the results will be multiplied by 2. The objective is not exactly to calculate the number of equipment, it is to determine the energy requirements for the process. Consequently, working with half of the flow and then multiplying is the correct approach.

Following the same procedure for half of the flow (185 Kg/s) the minimum diameter is 9,7 m and a lean MEA flow of 445 kg/s. The next step is to calculate the height of the absorption column. This will be done by reducing the height and increasing the lean MEA flow. Being the absorption an exothermic reaction, if there is a temperature profile, where the temperature does not change, means that the tower is not working properly, and has reached the minimum height. In the following picture, it can be seen the profile temperature for different values of height, absorbent flow, and diameters.

From Figure 14 can be seen that in the infinite length case (red dashed line), most of the length of the tower is not working (without causing any temperature change) because it is too long. The light blue lines represent other heights during the design process, the objective is to have a shorter column to reduce the initial investment. However, as a design rule, height/diameter should be always bigger than 1 (Madeddu et al., 2019). Based on that the height of 15 m and 10,15 meters of diameter is chosen, corresponding to a lean MEA flow of 547 Kg/s.

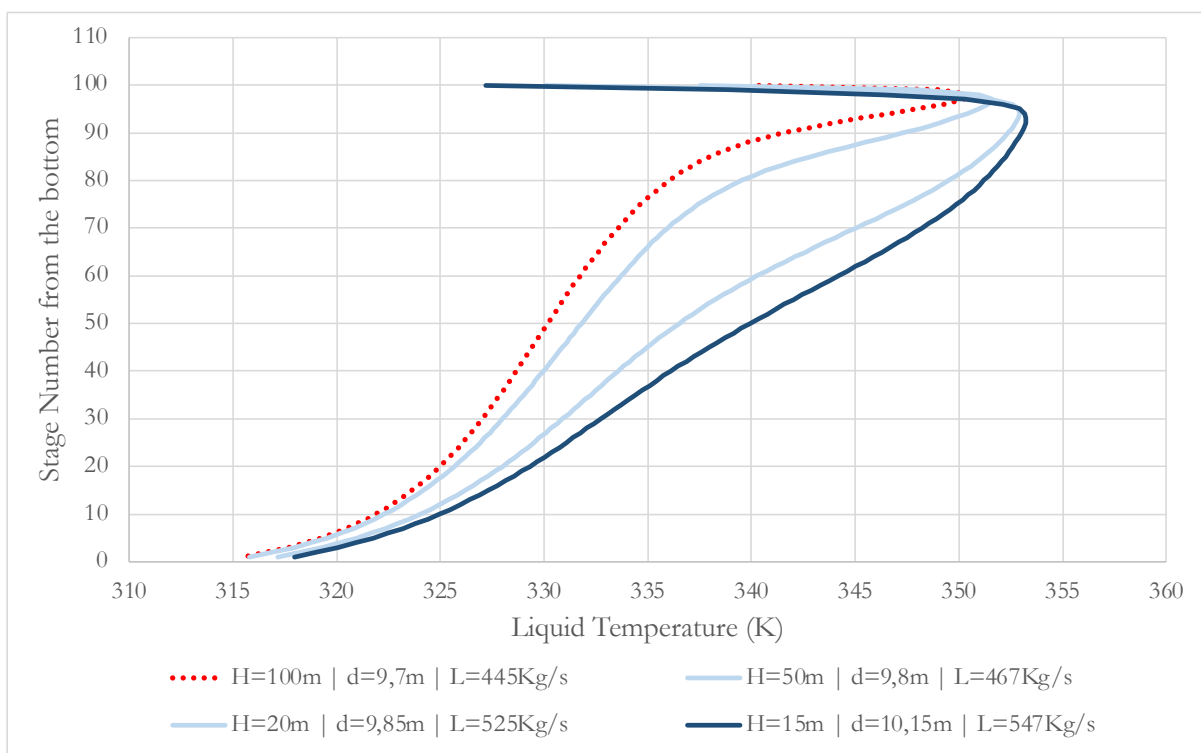


Figure 14: Temperature profile for different absorber heights

This behavior can also be seen in Figure 15 where the CO<sub>2</sub> molar fraction of the gas is plotted. It can be seen how the molar fraction remains unchanged in the first stages (top of the column) in the infinite case. It is good to notice that stage 100 (top) represents the outlet of the cleaned flue gas and 1(bottom) is the outlet of the CO<sub>2</sub>-rich amine (in liquid form).

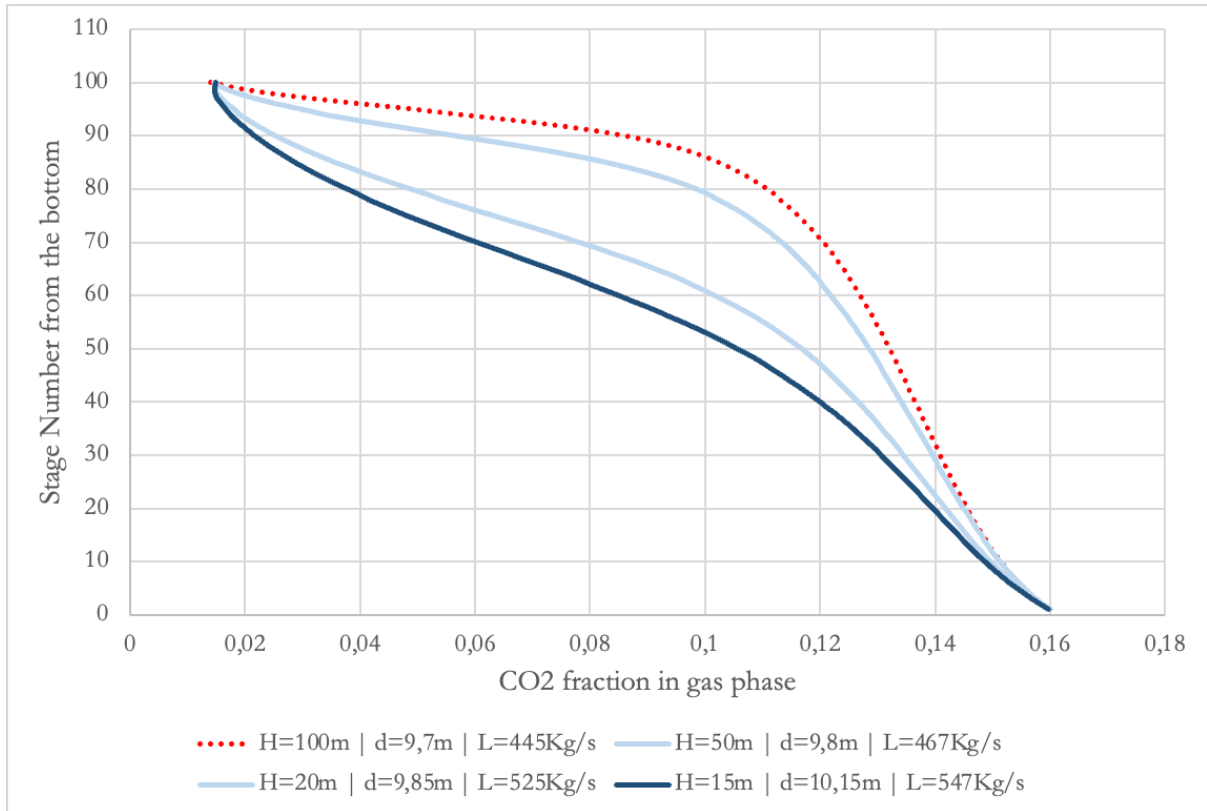


Figure 15: CO2 fraction for different heights

Finally Table 14 summarizes the results from the absorber dimensioning:

Number of units	2
Diameter	10,15m
Height	15m
Lean MEA mass flow rate	547 Kg/s
<b>Rich MEA</b>	
Mass flow rate	559 Kg/s
Temperature	45°C
Pressure	1 bar
mol CO2/mol MEA	0,522

Table 14: Absorber dimensioning main results

### 6.1.2 Stripper model for the RB

For the stripper dimensioning, the CO<sub>2</sub>-rich MEA flow and composition are fixed by the performance of the absorber, and the information on the rich MEA flow is shown in Table 14. The objective of the stripper is to remove the CO<sub>2</sub> from the MEA. Therefore, it will be dimensioned to achieve the same CO<sub>2</sub> concentration in the lean MEA as in the absorber, which is 5% of CO<sub>2</sub>, as shown in Table 11.

As explained before, the operational parameters were based on Madeddu et al., (2019). However, in Section 5.5 “Modeling the external components” the hot-rich MEA inlet temperature was not defined, which is the temperature after the recuperator in Figure 3. This temperature is determined

in the dimensioning of the recuperator, and as a design condition, it was chosen to be 2°C less than the saturation temperature at the operating pressure. Other parameters, such as geometry and reboiler duty, will be dimensioned in this section.

<b>Stripper</b>	
Hot Rich MEA inlet temperature	83°C
Operation pressure	1,8 bar
Pure CO <sub>2</sub> concentration after condenser	>98%
Lean MEA CO <sub>2</sub> concentration	5%
Condenser temperature	40°C
Reboiler duty	To be determined
Height	To be determined
Diameter	To be determined

*Table 15: Stripper dimensioning parameters*

As expected, for a fixed geometry, achieving cleaner lean MEA requires more energy in the reboiler. The dimensioning procedure involves selecting a stripper size (height and diameter) and then adjusting the reboiler duty until the exit lean MEA reaches 5% CO<sub>2</sub>. Once the CO<sub>2</sub> concentration is reached, the stripper size is reduced, and the reboiler duty is adjusted again. It has been found that the reboiler duty is almost the same for different stripper tower dimensions, as shown in the legend of Figure 16.

Figure 16 shows the liquid temperature profile, as for the absorber, the goal is to find the minimum size where the complete column works correctly. That means, as few isothermal zones as possible. It is seen how for 25 m height there is an isothermal zone in the middle of the column. It could be possible to reduce the height to even less than 9m. However, as a design rule, it was chosen that  $H/d > 1$ , so the diameter cannot be bigger than the height. Consequently the Stripper dimensions are  $H=9$  m,  $d= 7,4$  m, and a Reboiler duty of 161, 25 MW.

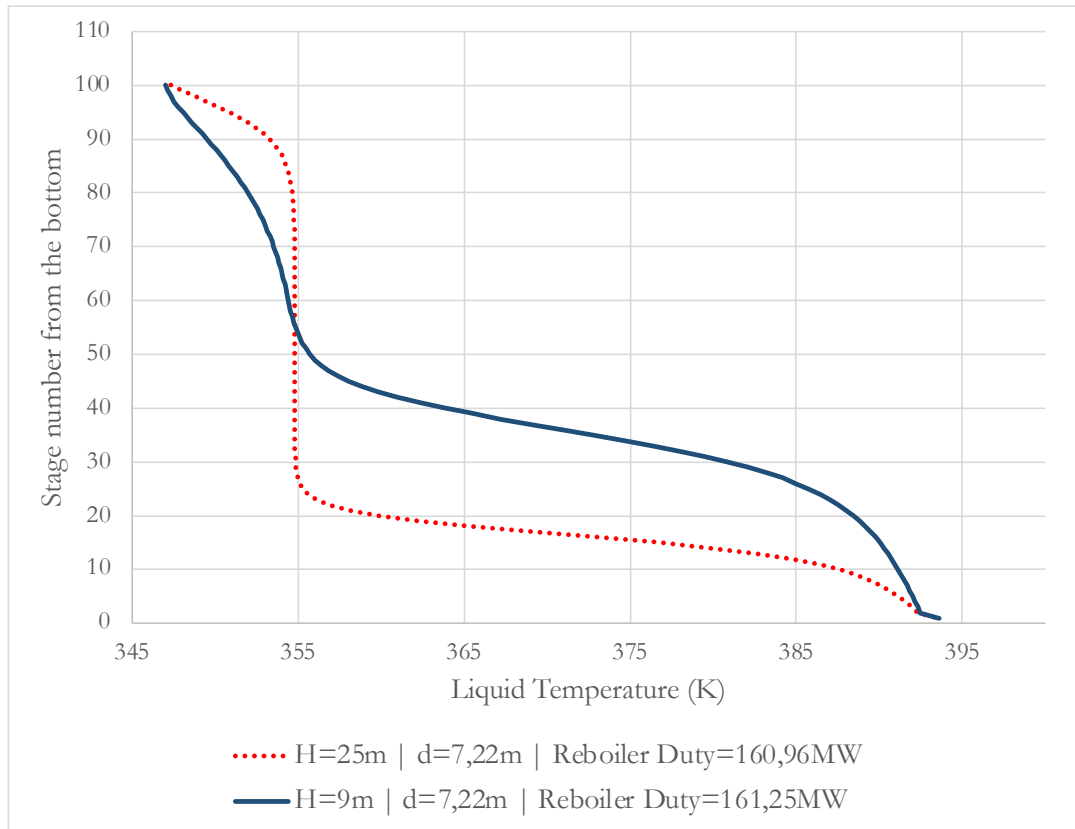


Figure 16: Stripper Temperature profile

### 6.1.3 MEA Cycle model for the RB

Once the Absorber and Stripper have been dimensioned, it is possible to join both columns. It is expected to have some change in the flow parameters and reboiler duty, due to the recirculation and makeup flows. Figure 17 represents the flowsheet for the MEA process including the main magnitudes (CO<sub>2</sub> balance, reboiler duty, and temperatures). It can be seen that some components have not been mentioned in detail before (pump, mixer, cooler, condenser, and recuperator) because these are heat exchangers, pressure changers, and mixers the dimensioning is straightforward and does not require further definition of other than, pressure and working temperature.

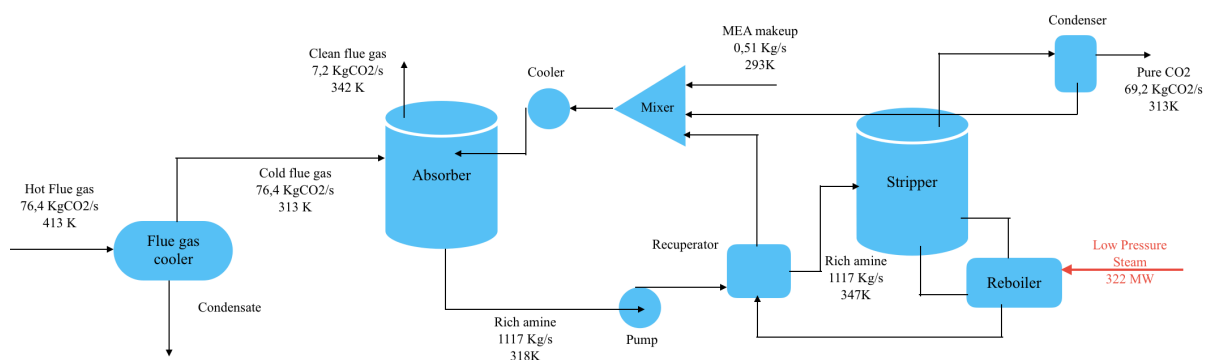


Figure 17: Standard MEA flowsheet

The final operational parameters for the MEA capture system can be seen in Table 16. Should be noted that there is a cooling duty associated with all the coolers and condensers of the process.

Furthermore, there is a small amount of electricity needed for the pump. It is worth mentioning that the compression of CO<sub>2</sub> has not been included in this study, but this would lead to a higher electricity requirement due to the compressors.

Inlet flue gas mass flow	370,000	Kg/s
Inlet CO <sub>2</sub> mass flow	76,368	Kg/s
Pure CO <sub>2</sub> produced mass flow	69,200	Kg/s
Lean solvent loading	0,23	molCO <sub>2</sub> /molMEA
Total heating duty	322,000	MW
Total cooling duty	369,760	MW
Electricity	0,104	MW
Capture efficiency (molar)	0,903	
Specific energy	4,670	MJ/Kg CO <sub>2</sub>

Table 16: Standard MEA process results

#### 6.1.4 Sensitivity analysis for the RB: Variation of the capture efficiency

The previous results show a specific energy of 4,67 MJ/KgCO<sub>2</sub>. In the next section, parameters such as the capture efficiency, stripper feed temperature (after recuperator in Figure 17), and operation pressure will be changed to see the impact on the specific energy. In the end, a new model will be done with the optimized parameters.

In the previous model, a value of 90% of capture efficiency was selected. This was because other researchers have used this value (Errico et al., 2016; Li B.H. et al., 2014; Madeddu, 2018). However, in this case, the energy requirements for different capture efficiency will be studied.

From Figure 18 can be seen how the reboiler duty increases linearly with the capture efficiency until a certain value around 90%. For higher values, there is a change in the slope of the graph, indicating that higher capture efficiencies would require a very large amount of energy for a very small improvement in the capture performance. Another important conclusion can be taken from Figure 19, where the specific energy has been plotted.

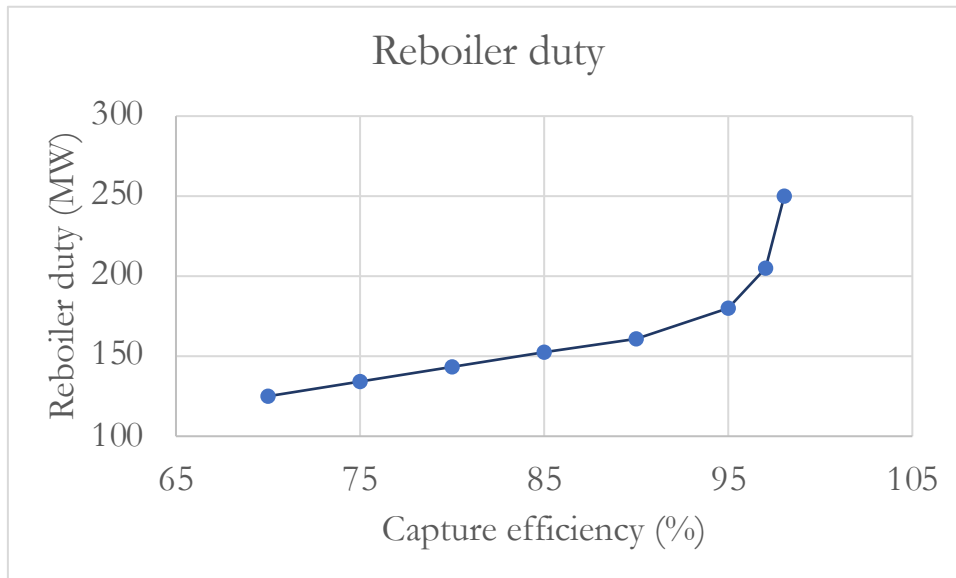


Figure 18: Variation of reboiler duty with capture efficiency

It can be seen how the specific energy (MJ/kg captured) remains practically constant until a certain value is around 90%. That means, that the capture efficiency can be increased to 90% without increasing the specific energy, the amount of reboiler duty only increases because of the higher rich solvent to be regenerated. Consequently, the capture efficiency remains unchanged and 90% is the chosen value.

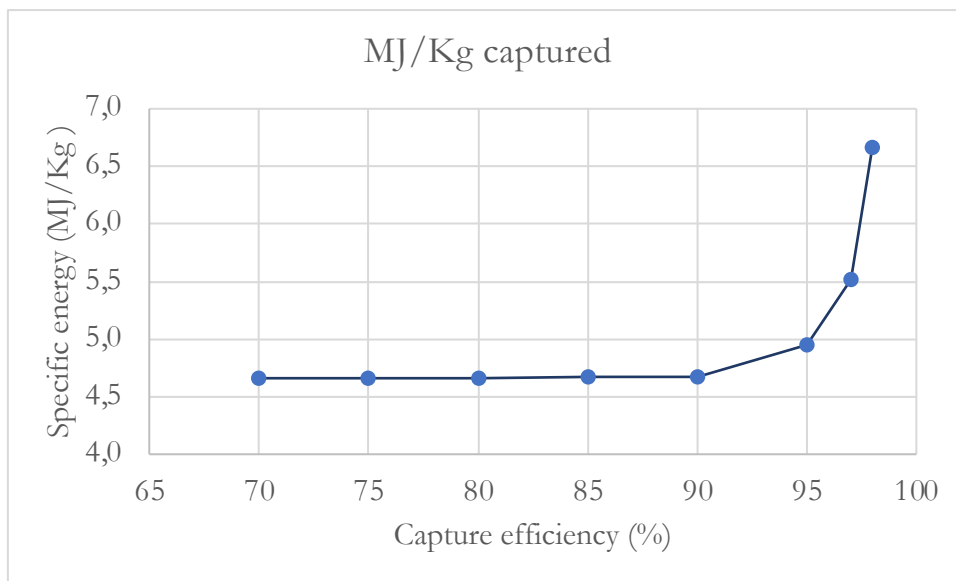


Figure 19: Variation of specific energy with capture efficiency

#### 6.1.5 Sensitivity analysis for the RB: Variation of stripper inlet temperature

Being the regeneration is an endothermic reaction, it is expected that when increasing the temperature of the rich amine inlet to the stripper the energy needed in the reboiler will be less.

As a design consideration of the recuperator from Figure 17, the minimum temperature difference between the hot stream (lean solvent) and cold stream (rich solvent) is defined as 10°C. In all the heat exchanger zones, the hot stream should always be 10°C higher than the cold stream. Having said that the temperature has been evaluated in the two temperatures shown in Table 17.

T feed stripper (K)	Reboiler Duty (MW)	MJ/Kg captured
347	161	4,67
375	125	3,61

Table 17: Variation of stripper inlet temperature

As can be seen, the reboiler duty has been reduced by 23 % of the original value with a temperature of 375K of the stream feeding the stripper in Figure 17. The following Figure 20, illustrates the new temperature profile of the stripper. As explained by Madeddu et al., (2019) with higher inlet temperature, there are more isothermal zones, which can be seen as a potential for reduction of the column size.

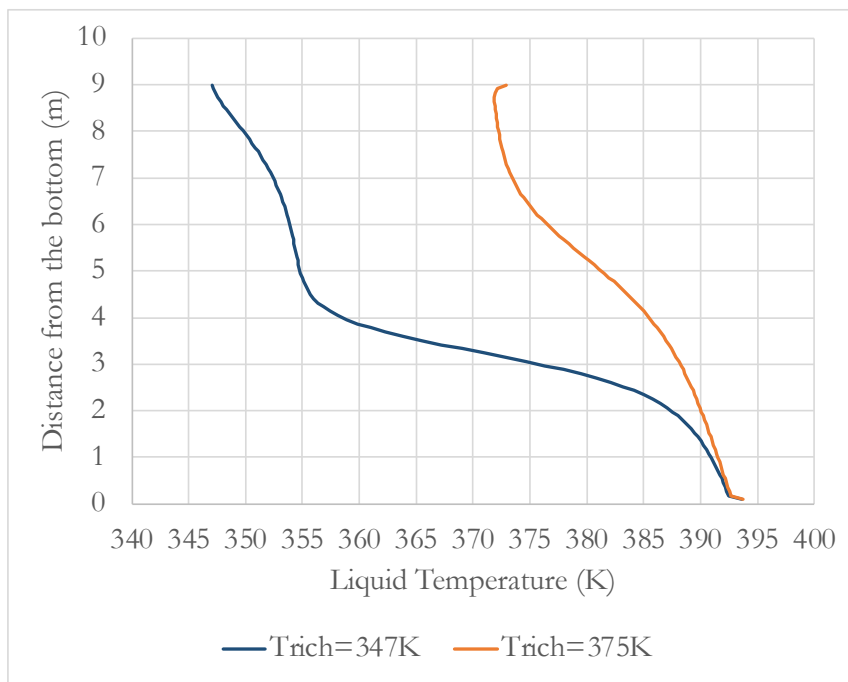


Figure 20: Variation of the liquid temperature profile of the stripper with the inlet temperature

#### 6.1.6 Sensitivity analysis for the RB: Variation of stripper operation pressure

The operating pressure of the stripper has been changed to analyze its impact on the reboiler duty. Figure 21 shows that increasing the stripper pressure leads to a reduction in the reboiler duty. As mentioned in Section “2.1.1 MEA,” one component of the reboiler duty is the stripping heat, which is essentially the heat needed to produce the steam that strips the CO<sub>2</sub> out of the column. If there is more CO<sub>2</sub> in the gaseous form, less stripping steam is needed, and consequently, the reboiler duty is reduced.

As explained by Warudkar et al. (2013), the partial pressure of CO<sub>2</sub> increases faster with temperature than H<sub>2</sub>O. With higher pressure, there is a higher temperature; hence, more CO<sub>2</sub> is in the gas phase. Consequently, less energy is needed to strip the CO<sub>2</sub> from the rich mixture.

Increasing the pressure also implies increasing the operation temperature of the reboiler. The temperature has two limitations, firstly, there is a temperature limit for the MEA degradation which is around 120 °C (Zhou et al., 2012), and secondly, higher reboiler temperatures indicate higher steam temperature/pressure in the reboiler, hence, higher energy losses from the power production point of view.

Additionally, at lower pressure the specific volume increases. Consequently, it is needed to increase the column diameter to maintain the same mass flow, without reaching the flooding velocity (Madeddu, 2018). Finally, the chosen operational value is 1,8 bar. As highlighted in Figure 21 is the pressure value where the maximum allowable operation temperature is reached.

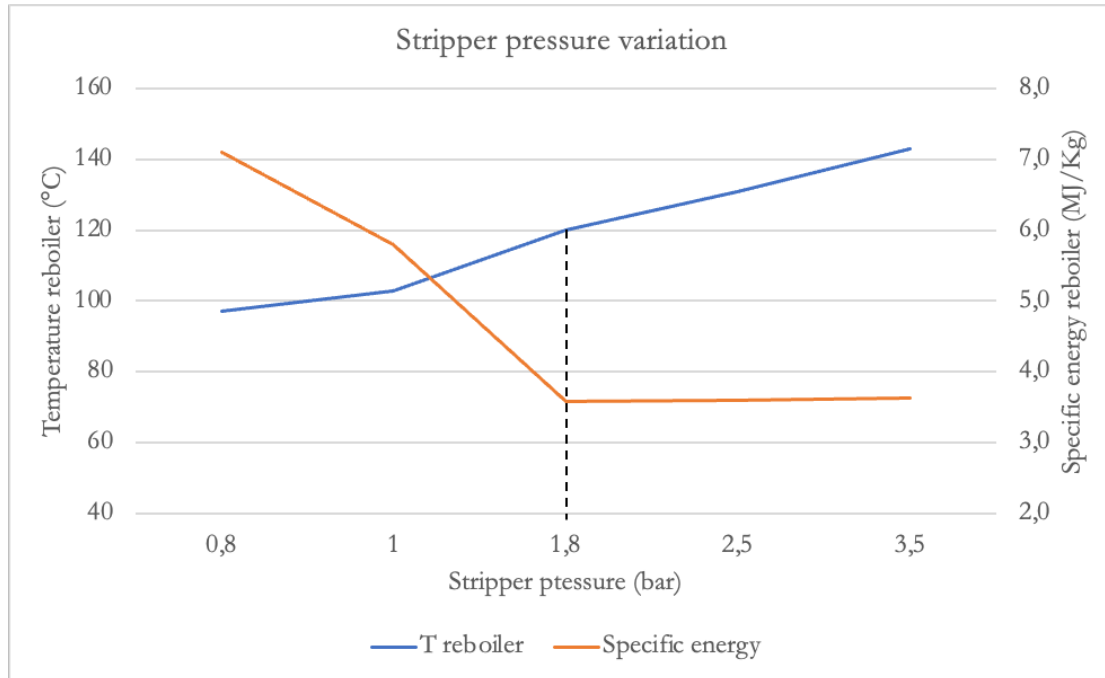


Figure 21: Variation of the reboiler temperature with the stripper pressure

## 6.2 Final MEA process for the RB

Finally, the results from using optimized operational parameters are presented in Table 18. The parameters that have been adjusted or validated at the optimal point were the ones studied in the previous sensitivity analysis.

Inlet flue gas mass flow	370,000	Kg/s
Inlet CO <sub>2</sub> mass flow	76,368	Kg/s
Pure CO <sub>2</sub> produced mass flow	69,200	Kg/s
Lean solvent loading	0,23035	molCO <sub>2</sub> /molMEA
Total heating duty	250,000	MW
Total cooling duty	280,534	MW
Electricity	0,092	MW
Capture efficiency (molar)	0,904	
Specific energy	3,613	MJ/Kg CO <sub>2</sub>

Two units		
	Absorber	Stripper
<b>Diameter (m)</b>	10,15	7,22
<b>Height (m)</b>	15	9

Table 18: Final MEA CC parameters for the Recovery Boiler

### 6.3 Final MEA process for the LK

For the LK, the model has been done directly utilizing the same procedure and parameters used for the RB. The final results of the carbon capture process are shown in Table 19.

Inlet flue gas mass flow	42,000	Kg/s
Inlet CO <sub>2</sub> mass flow	12,050	Kg/s
Pure CO <sub>2</sub> produced mass flow	10,820	Kg/s
Lean solvent loading	0,23529	molCO <sub>2</sub> /molMEA
Total heating duty	39,230	MW
Total cooling duty	55,240	MW
Electricity	0,015	MW
Capture efficiency (molar)	0,9	
Specific energy	3,626	MJ/Kg CO <sub>2</sub>

	Absorber	Stripper
<b>Diameter (m)</b>	6	5
<b>Height (m)</b>	10	6

Table 19: Final MEA CC parameters for the Lime Kiln

### 6.4 Impact of CC in the mill

In this section, the impact of CC will be discussed in the case of no process integration. That means only utilizing LPS (Low-Pressure Steam) extracted from the turbine as a heat source for the reboiler. The base case of the mill, without carbon capture, is presented in Table 20.

<b>High Pressure Steam (HPS) Temperature</b>	494°C
<b>High Pressure Steam (HPS) Pressure</b>	94,8 barg
<b>Power production TG1 (MW)</b>	89
<b>Power production TG2 (MW)</b>	88
<b>Power consumption (MW)</b>	90
<b>Power to the grid (MW)</b>	87
<b>CO<sub>2</sub> emitted (Kg/s)</b>	88,418

Table 20: Mill base case without carbon capture

Where it needs to be reminded that TG1 is the back pressure turbine and TG2 the condensation turbine.

According to Table 18 if 90% of the CO<sub>2</sub> present in the flue gas from the RB is meant to be captured it is needed to supply 250 MW at a temperature higher than 120°C. The LPS is at 4 bar(g), considering a saturation temperature of 152 °C, it is enough to work as a heat source.

To supply the 250 MW and neglecting the sensible heat (only considering latent heat), the amount of steam is given by Equation (17).

$$\dot{m}_{\text{steam}} = \frac{250}{h_{\text{fg}@4\text{barg}}} = 118,62 \frac{\text{Kg}}{\text{s}} \quad (17)$$

Based on information received by Mdp the total amount of available Low-Pressure Steam (LPS) is around 60 Kg/s, meaning that there is not enough steam for the CC implementation in the RB. Considering that only 50 Kg/s can be extracted because there is a minimum flow requirement in the condenser. With that amount of available steam, it is possible to capture 29 Kg/s of CO<sub>2</sub>, which represents 38% of the RB CO<sub>2</sub> emissions. However, this available LPS can be used for implementing CC for the lime kiln. In the case of the LK using Equation (17) for the total heating duty of 39,23 MW the amount of LPS needed is 18,61 Kg/s.

Increasing the LPS extraction has an impact on power generation, less electricity is produced because there is less steam in the last stages of the turbine. To calculate the power loss, the overall isentropic efficiency needs to be assumed.

Assuming an overall isentropic efficiency of 0,86 (Genrup, 2023) the enthalpy of the exhaust steam from the turbine can be calculated using Equation (18).

$$\eta_s = (h_1 - h_3)/(h_1 - h_{3s}) \quad (18)$$

Where:

$\eta_s$ : Overall isentropic efficiency

$h_1$ : Inlet enthalpy @ 94,8 bar(g) and 494°C

$h_3$ : Real outlet enthalpy @ - 0,9 bar(g)

$h_{3s}$ : Isentropic enthalpy @ - 0,9bar(g) and  $s = s_1$

Consequently  $h_3 = 2269,32 \frac{\text{kJ}}{\text{kg}}$  @  $T = 319 \text{ K}$ . For the low-pressure extraction, there is no need to do any calculation because there is a pressure and temperature measure in the mill and the enthalpy value is  $h_2 = 2777,01 \frac{\text{kJ}}{\text{kg}}$ . Finally, the loss in power generation is given by Equation (7) assuming a mechanical efficiency of 0,99 (Genrup, 2023).

$$\text{Power loss} = \dot{m}_s * (h_2 - h_3) * \eta_m \quad (19)$$

Where:

$\dot{m}_s$ : Is the steam massflow needed for CC

$\eta_m$ : Mechanical efficiency

In order to capture 38% of the CO<sub>2</sub> from the RB, there is a reduction in the power generation of 23,15 MW. For the case of capturing the flue gases for the LK the loss in power generation will be 9,35 MW. The results of the power balance without process integration are shown in Figure 22.

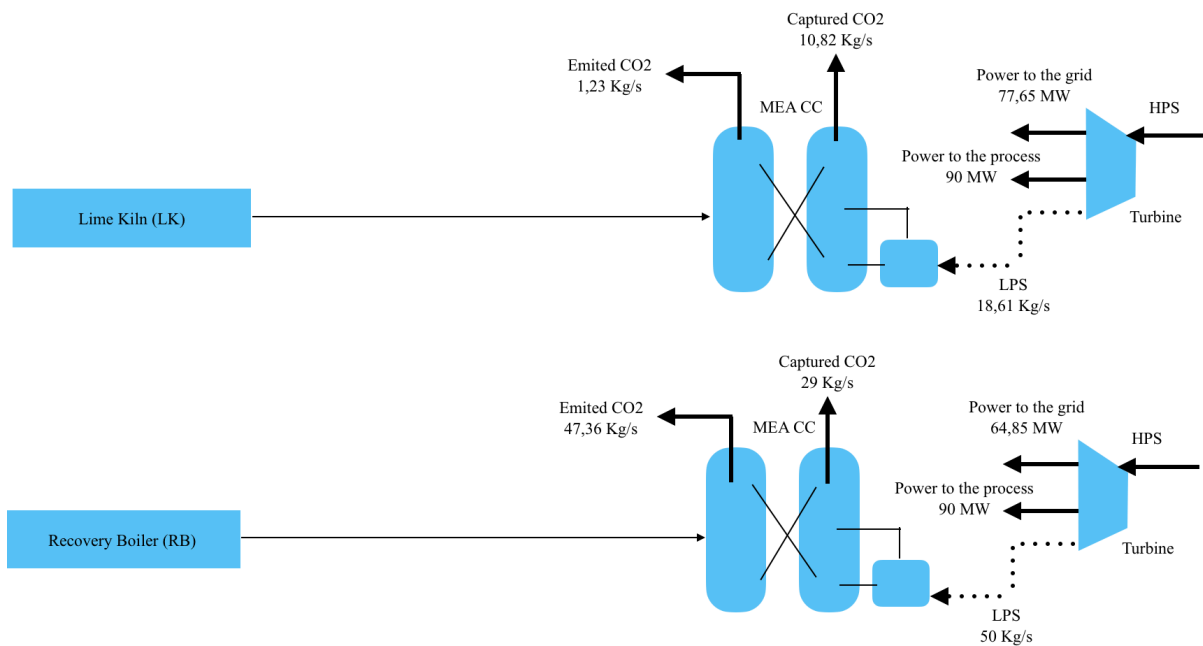


Figure 22: Carbon Capture without process integration

It should be mentioned, that the CC system has been dimensioned for capturing 90% of the CO<sub>2</sub> content in the flue gases. In the case of the RB it is only possible to capture 38% of the CO<sub>2</sub> content, hence, knowing that information, the absorber and stripper could be redimensioned to reduce the diameter and height.

## 7 Process integration study

There are several ways of heat integration. The common ones are the utilization of heat exchangers, always respecting a minimum difference between cold and hot streams. Consequently, in the case of using waste heat for the reboiler, it will be needed to have a temperature level above 130°C at the outlet of the reboiler. In the pulp mill operation, the only waste heat source at that temperature is the flue gases. In cases where that temperature level is not available, heat pumps can be implemented.

The utilization of hot-temperature heat pumps reduces the need for such high-temperature sources and other sources of less temperature can be used. This can be done, by the working principle of the heat pump, where the penalty is the electricity required to run the compressor. However, the implementation of high-temperature heat pumps at a large scale is not completely adopted by the pulp and paper industry at the moment.

Additionally, to the utilization of heat pumps or heat exchangers directly for the carbon capture process, other alternatives can be analyzed to reduce the steam consumption of the pulp production process and have more steam available for the CC. To identify the opportunities for steam saving, a complete energy-efficient analysis of the process should be done, this would require measuring all the heat-exchanging streams of the mill, with flows and temperature.

An energy efficiency analysis was done by Pedersén and Larsson at the Södra Cell Värö mill in 2017. As it was said in the literature review, in that analysis steam saving opportunities are suggested by the utilization of a pinch analysis and identification of pinch violations. For this thesis, only one of these steam-saving suggestions will be studied in the specific case of MDP.

Finally, the process integration study will be divided into three sections:

- Use flue gas energy as a heat source for CC
- Use medium-temperature waste heat (warm and hot water) as a heat source in a heat pump to be used in CC
- Steam saving option:
  - Use warm water and hot water to preheat combustion air in the RB and increase steam availability

The 3 study cases can be seen in Figure 23. In light blue, the standard process component of the MEA CC and the mill. In red, it is indicated the recovery of the heat from the flue gases. It will be mentioned later that only the heat from the LK can be recovered. In green the implementation of steam generation heat pumps, for the RB or the LK the heat pumps are different, due to the differences in the steam demand. Finally, purple represents the integration of a water/air preheater to reduce the consumption of medium-pressure steam and then have more steam availability for the CC process.

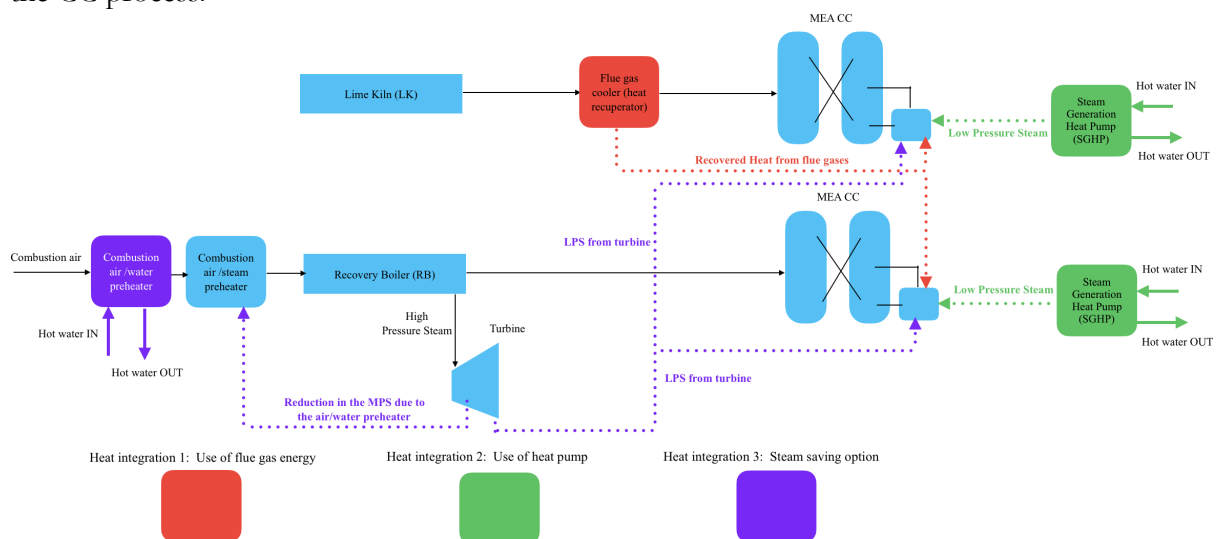


Figure 23: Process integration study cases

## 7.1 Use flue gas (FG) in CC

The FG from the RB has a flow of 370 Kg/s with a temperature before FGC (Flue Gas Cooler) of 220°C, from the PB (Power Boiler) the flow is 28,6 Kg/s with a temperature of 160°C, for the LK the flow is 41,77 Kg/s and temperature of 280°C. In the case of the RB, nowadays the FG is cooled in the FGC to a temperature of 130°C exchanging heat with the feed water. Hence, the energy from the flue gases of the RB is already used and it is not available. However, flue gas cooling is available from the lime kiln.

For the PB and LK the energy available is presented in Table 21. The cold temperature of the FG is set to 130°C assuming a minimum temperature difference of 10°C.

	Mass flow (Kg/s)	Temperature in (°C)	Temperature out (°C)	Available heat (MW)
FG from PB	29	160	130	0,9
FG from LK	42	280	130	6,7

Table 21: Flue Gas available energy

From the above table, the FG from PB will be neglected and not considered in the heat integration. Assuming that the 6,7 MW are available for utilization in the CC of the RB and LK.

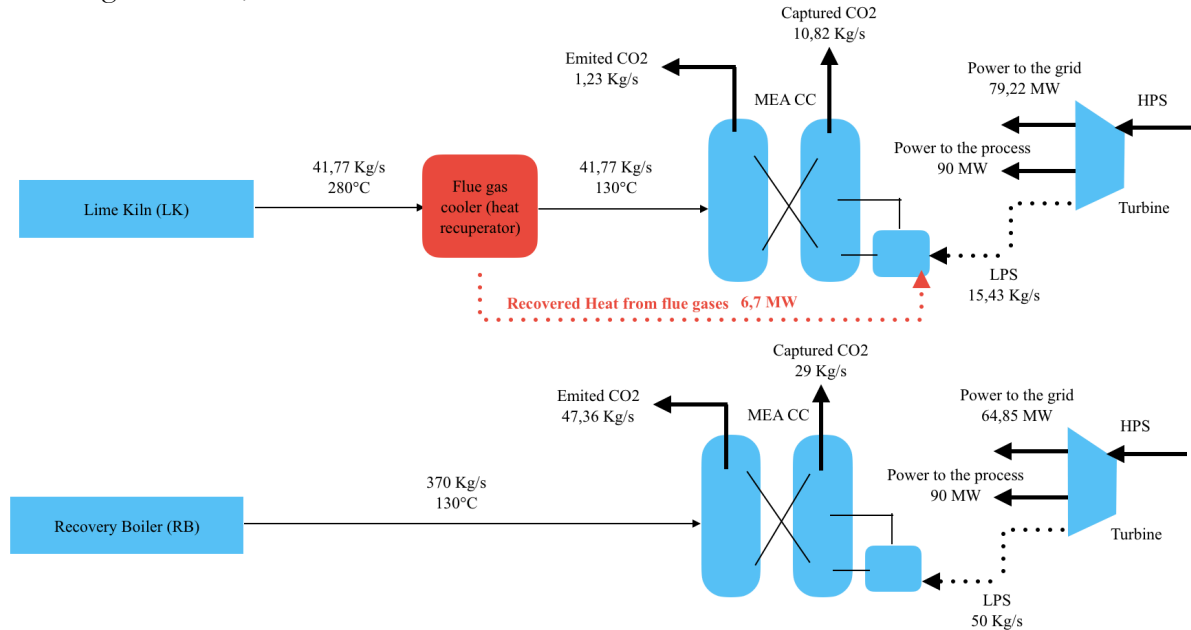


Figure 24: Flue gas cooling flowsheet

Figure 24 summarise the results. If the FG is used in the reboiler when capturing the CO<sub>2</sub> from the LK, only 32,53 MW would be needed, representing 15,43 Kg/s of LPS hence only 7,76 MW reduction in the generation of the turbine. In the case of the RB, 6,7 MW represents 2,7% of the total energy demand, so the impact of utilizing this energy will be neglected.

## 7.2 Heat pumps for hot and warm water streams

One important hot water stream that could potentially be used is the return of the cooling water from the scrubber of the dissolving tank vent. The estimated flow is around 120 l/s with a temperature of 85°C. The temperature level is not enough to be used in the reboiler. Hence, a high-temperature heat pump (HTHP) or a steam generation heat pump (SGHP) needs to be used.

There are several studies in the field of HTHP and SGHP (Jiang et al., 2022; Klute et al., 2024; Koundinya et al., 2023). Furthermore, some important companies have such heat pumps in their portfolio. In general, the COP (Coefficient of Performance) of an industrial SGHP is between 2 and 3 (Siemens, 2023) The dimensioning of the heat pump in this thesis will be based on standard parameters found during the literature review. The main goal of this section is to analyze if an SGHP is thermodynamically possible and can generate energy savings in the CC implementation.

The working principle of SGHP is shown in Figure 25. This working principle is commercially available (Fuji, 2022) and an adapted model has been done by Koundunya et al., (2023) for the low-pressure steam generation. In the mentioned papers, the focus is on the design of the compressor and the study of different refrigerants. For the sake of simplicity, in this thesis, the heat pump will be modeled as a standard heat pump with the addition of one flash tank, as the

commercial option of Siemens and Fuji Technology. The HW (Hot Water) will be used as a heat source and the WW (Warm Water) as a heat sink. The objective is to heat the Warm Water OUT stream until the desired temperature level (135 °C) and then flash that stream to produce low-pressure steam (3 bar).

For CC in the LK and RB the size of the heat pump will be different. In the case of the RB it is needed to produce 115,6 Kg/s of steam in the flash tank conditions (135°C, 3 bar) and 18,13 Kg/s for the LK. The refrigerant will be R1233zd which has a high critical temperature (166,45°C) (Koundinya et al., 2023). The maximum allowed temperature after the compressor is limited to 150°C (Koundinya et al., 2023). As before, the minimum temperature difference for the heat exchangers is set to 10°C.

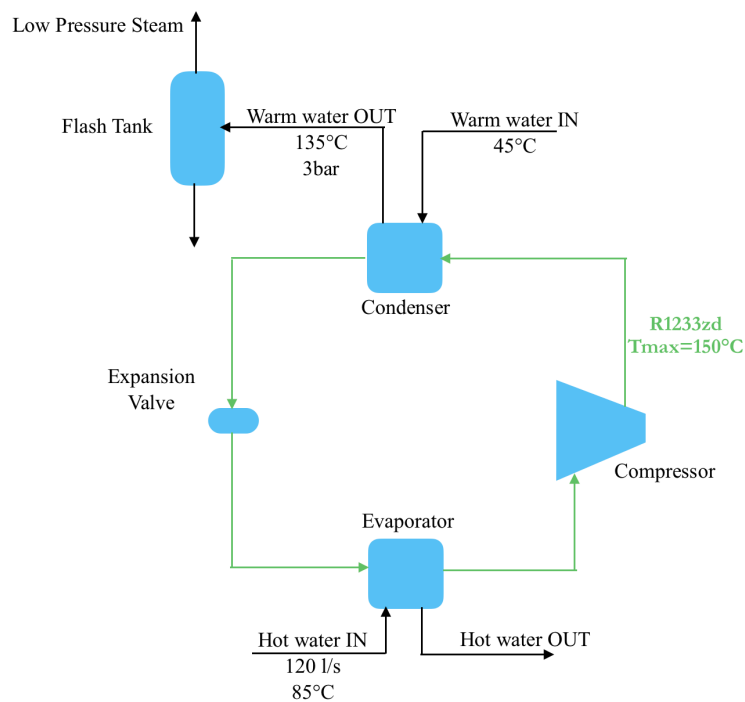


Figure 25: Model of SGHP

Table 22 shows the heat pump parameters when maximizing the steam generation. According to the modeling of the SGHP, the maximum steam is 60 Kg/s, the main restriction is the minimum temperature difference in the condenser. It can be seen how the HW leaves the evaporator at 57°C, the only option to reduce even more that temperature (use more waste heat) is to increase the refrigerant flow and that will lead to an increase in the work of the compressor hence less COP, because the heat extracted in the condenser is the most restrictive condition (minimum of 10°C).

Refrigerant flow	150 Kg/s
Compressor pressure	12 bar
HWIN	85 °C
HWOUT	57 °C
WWIN	45 °C
WWOUT	135 °C
Steam generation	60 Kg/s
<b>Power input</b>	<b>9,053 MW</b>
<b>Thermal power output</b>	<b>22,742 MW</b>
<b>COP</b>	<b>2,51</b>
<b>Power available in the steam</b>	<b>139,8 MW</b>

*Table 22: Maximum Steam production with the SGHP*

From the above table, it can also be seen that there is not enough energy in the generated steam still a huge amount of LPS (52,3 Kg/s) needs to be extracted from the turbine. In the case of the LK, the dimensioning parameters are shown in Table 23, the size of the heat pump is much smaller and the steam generated is enough for the carbon capture module without extra steam.

Refrigerant flow	55 Kg/s
Compressor pressure	12 bar
HWIN	85 °C
HWOUT	76 °C
WWIN	45 °C
WWOUT	135 °C
Steam generation	20 Kg/s
<b>Power input</b>	<b>3,319 MW</b>
<b>Thermal power output</b>	<b>7,581 MW</b>
<b>COP</b>	<b>2,28</b>
<b>Power available in the steam</b>	<b>46,58 MW</b>

*Table 23: SGHP Parameters for capturing CO<sub>2</sub> from the lime kiln*

Figure 26 summarize the impact on the mill when SGHP is implemented.

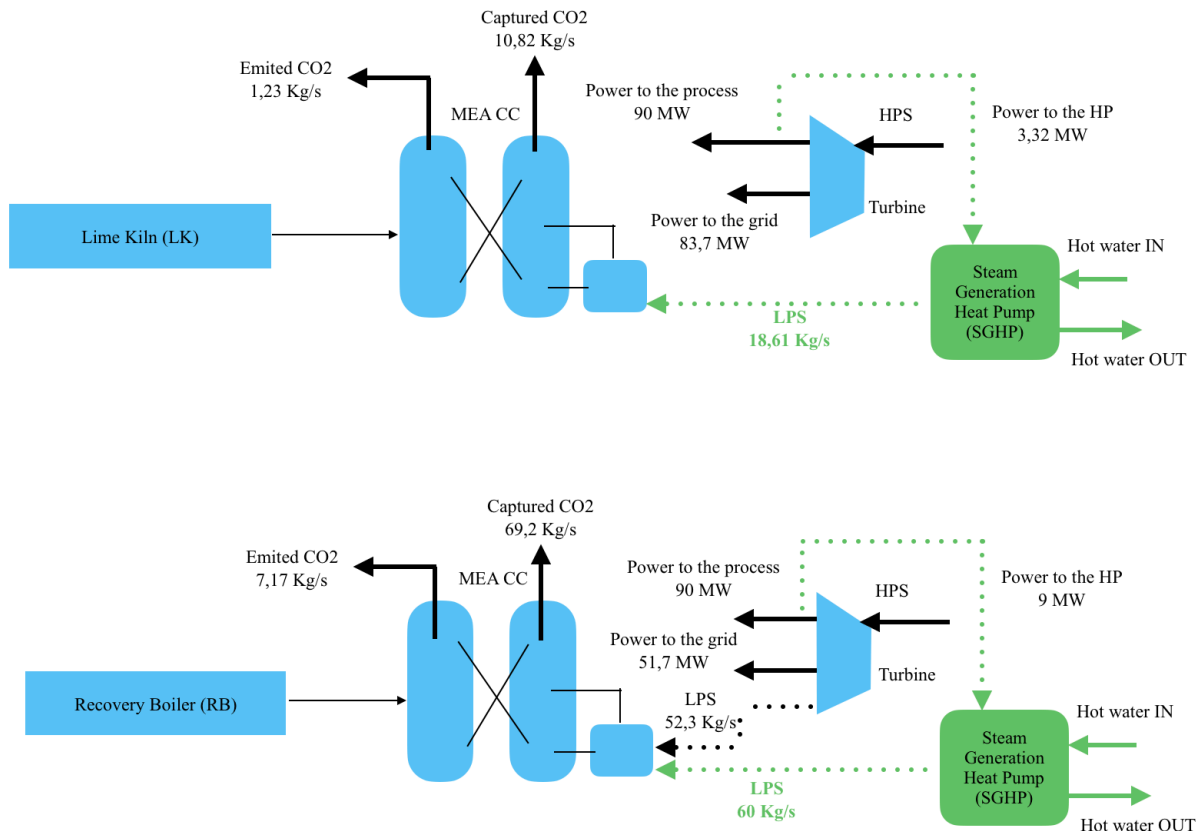


Figure 26: Waste heat valorization flowsheet

### 7.3 Hot water (HW) to preheat combustion air in the RB

Currently, the combustion air is preheated by utilization of LPS and medium-pressure steam (MPS). The temperature set after the air preheaters is 150°C. In this section, HW will be analyzed as a heat source in the preheating of air. It is already known that the temperature level will not be enough for the total temperature increase of air, because hot water is at 85°C. Despite that, the utilization of that stream can partly reduce steam consumption.

By design, the LPS and MPS consumption is 10,5 Kg/s and 7,95Kg/s respectively. The ambient temperature is 30°C and the outlet temperature is 150°C. Without a distinction between primary, secondary and tertiary air Figure 27 represents the heating process of a design total airflow of 295,64 Kg/s. The outlet temperature of the combustion air is higher than 150 °C because no losses were considered in the model.

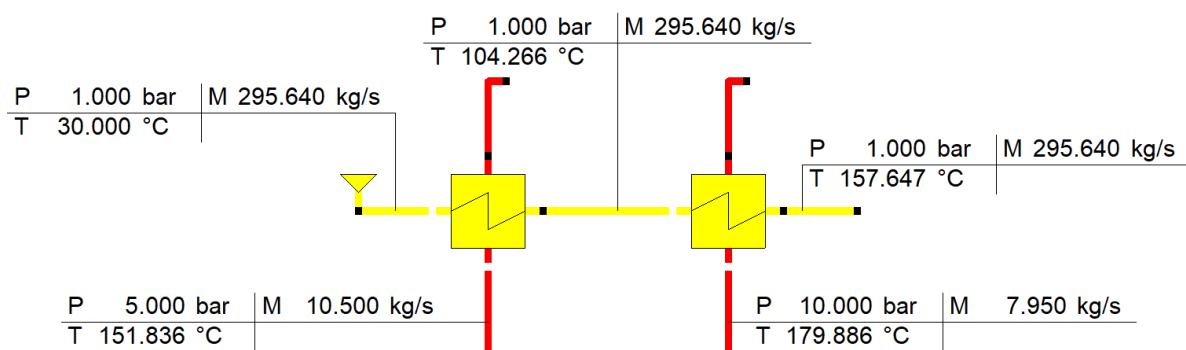


Figure 27: Simplified current combustion air preheating system

In the previous configuration, the steam leaves the preheater as saturated water. Only condensation heat is used. With that configuration, the difference in temperature between the inlet of steam and the outlet of water is around 50°C for the low-pressure heater and 22°C for the medium-pressure heater. An estimation of the heat exchange area is 6166 m<sup>2</sup> for the LPS air preheater and 8081 m<sup>2</sup> for the MPS air preheater.

Adding a new water-air heat exchanger before the steam-air preheaters and reducing the upper-temperature limit to 10°C the configuration will consume less LPS and MPS. The new steam consumptions are seen in Figure 28. Comparing both figures the steam saving is 5,75 Kg/s MPS and 1.1 Kg/s LPS. However, as expected, there is a substantial area increase. The LPS air-preheater requires now 13968 m<sup>2</sup>, the MPS air preheater 6722 m<sup>2</sup>, and the new water-air exchanger 16733 m<sup>2</sup>.

By getting rid of the 10°C difference, and allowing the outlet steam to leave the exchanger at condensation temperature, the area of the MPS air-preheater can be reduced to around 3253 m<sup>2</sup>, without having a significant impact on the air outlet temperature. When evaluating a real project, not only the operation cost (steam consumption) should be optimized, but the initial investment (exchange area) should be considered as well. Figure 28 shows the new configuration, with a reduction in steam consumption and an increase in the exchange area.

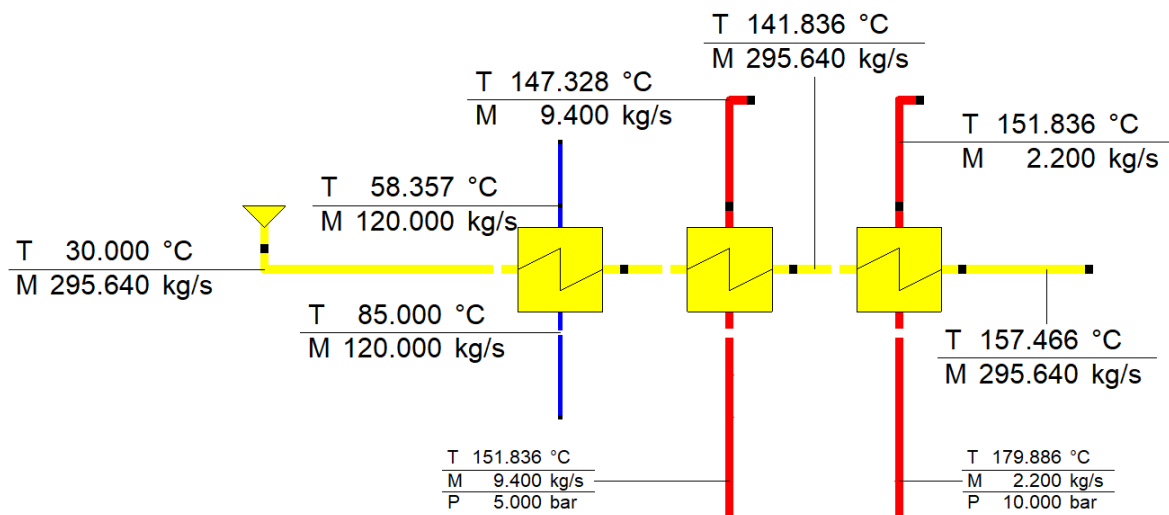


Figure 28: Proposed air preheating system

For the CC it is not needed to use MPS, hence the 5,75 Kg/s can be expanded until the end of the turbine ( $h_3$  from Equation (18)), generating increasing electricity production as given by Equation (20). The conditions of MPS are known, 10 bar(g) and 222°C, having an enthalpy of 2179kJ/Kg

$$\text{Increase in power production} = \dot{m}_{\text{saved}} * (h_{\text{MPS}} - h_{\text{out}}) * \eta_m = 3,5 \text{ MW}. \quad (20)$$

The total amount of saved steam rose to 6,86 Kg/s of LPS. That steam represents only 5,7% of the steam needed in the RB, so the impact will be neglected. Si still there is not enough steam for increasing the capturing rate in the RB. The new power balance is summarized in Table 24, where the increase in power production from Eq (20) has been considered.

Integration 1: LK Flue gas valorisation			
Integration 2: Stem Generation Heat Pump			
Integration 3: New air preheater			
		<b>Integrction 3</b>	
	<b>No CC</b>	<b>RB*</b>	<b>LK</b>
<b>Power to the grid (MW)</b>	87,0	67,4	81,2
<b>CO2 emitted by source (Kg/s)</b>	88,4	47,4	1,2
<b>Total CO2 emitted (RB+LK)(Kg/s)</b>	88,4	59,4	77,6
<b>CO2 captured (Kg/s)</b>	0,0	29,0	10,8

\* The steam saved is neglected for capturing the CO<sub>2</sub> from the RB.

Table 24: Power balance with the new air preheating system

## 7.4 Summary

Multiple scenarios were analyzed for the process integration study. The main results of each case are illustrated in Table 25. Firstly, it was demonstrated that the energy content of the flue gases reduces 5,7% of the steam needs when capturing the CO<sub>2</sub> from the LK. The impact on the RB was negligible. This is primarily due to the small flue gas flow of the LK.

Integration 1: LK Flue gas valorisation									
Integration 2: Stem Generation Heat Pump									
Integration 3: New air preheater									
		<b>No integration</b>		<b>Integrction 1</b>		<b>Integrction 2</b>		<b>Integrction 3</b>	
	<b>No CC</b>	<b>RB</b>	<b>LK</b>	<b>RB*</b>	<b>LK</b>	<b>RB</b>	<b>LK</b>	<b>RB*</b>	<b>LK</b>
<b>Power to the grid (MW)</b>	87,0	63,9	77,7	63,9	79,2	51,6	83,7	67,4	81,2
<b>CO2 emitted by source (Kg/s)</b>	88,4	47,4	1,2	47,4	1,2	7,2	1,2	47,4	1,2
<b>Total CO2 emitted (RB+LK)(Kg/s)</b>	88,4	59,4	77,6	59,4	77,6	19,2	77,6	59,4	77,6
<b>CO2 captured (Kg/s)</b>	0,0	29,0	10,8	29,0	10,8	69,2	10,8	29,0	10,8

\* The steam saved is neglected for capturing the CO<sub>2</sub> from the RB.

Table 25: Summary of results

An important finding is that utilizing an SGHP is the only method capable of capturing 90% of the CO<sub>2</sub> emitted by the RB. Even though employing the heat pump necessitates a significant amount of direct steam from the turbine, along with the power consumed by the compressor, there is a reduction in the energy injected into the grid by 35.3 MW. In the case of the LK, the reduction is only due to compressor consumption, as no direct steam from the turbine is required, resulting in a reduction of only 3.3 MW.

Furthermore, implementing a water-air preheater has the potential to save a considerable amount of energy by reducing MPS consumption. While the electricity injected into the grid could potentially increase by around 3,5 MW, the mass flow of saved steam does not significantly impact the carbon capture process.

It is important to highlight that the minimum upper terminal temperature difference for the heat exchangers has been defined as 10°C. In a more detailed study, it would be advisable to explore different values of temperature difference based on the fluids and exchanging conditions.

## 8 Conclusions

It can be said that this study provides answers to the research questions posed in Chapter 1. The energy requirement for the implementation of MEA (Monoethanolamine) carbon capture is 3.6 MJ/kgCO<sub>2</sub>, a value consistent with findings in the literature and commercial applications. As previously mentioned, the energy requirement is dependent on the carbon capture technology,

with MEA being the most common and the one modeled in this study. This value can serve as a benchmark for comparison when evaluating novel technologies such as Enzymatic carbon capture.

Regarding the second research question, the study reveals that there is no straightforward method to install the carbon capture module without reducing the energy injected into the grid. This is not only due to the specific energy requirements in the stripper but also the significant flue gas flow of the recovery boiler. However, the utilization of a steam generation heat pump could potentially provide a solution for waste heat valorization and reduce the direct steam needed in the stripper.

Finally, if the mill decides to implement a carbon capture process, it would be advisable to start by capturing CO<sub>2</sub> from the lime kiln using a steam generation heat pump. This approach would minimize the impact on the mill. As an initial investment in new technology, it would be prudent to begin with smaller equipment with lower energy consumption. Furthermore, based on market research and assumptions made, it appears that a portion of the CO<sub>2</sub> demand can be met with CO<sub>2</sub> from the lime kiln.

As a final recommendation, it could be beneficial to conduct an energy efficiency study of the mill utilizing pinch analysis. This method can help identify waste streams and potential reductions in energy consumption. Additionally, it may identify other waste streams, potentially allowing the steam generation heat pump to produce more steam than calculated in the thesis.

## 9 References

- Aaron, D., Tsouris, C., 2005. Separation of CO<sub>2</sub> from Flue Gas: A Review. *Sep. Sci. Technol.* 40, 321–348. <https://doi.org/10.1081/SS-200042244>
- ACCSESS, 2022. SP1: CO<sub>2</sub> Capture Piloting – Access. URL <https://www.projectaccess.eu/sp1-co2-capture-piloting>
- Adu, E., Zhang, Y.D., Liu, D., Tontiwachwuthikul, P., 2020. Parametric Process Design and Economic Analysis of Post-Combustion CO<sub>2</sub> Capture and Compression for Coal- and Natural Gas-Fired Power Plants. *Energies* 13, 2519. <https://doi.org/10.3390/en13102519>
- Agency, C.-E.C., Infrastructure and Environment Executive, 2024. Industrial Carbon Management: Interactive Stories [WWW Document]. ArcGIS StoryMaps. URL <https://storymaps.arcgis.com/stories/1fcc606673dc4df7ac54cf0a1db8dd93>
- Arango Munoz, P., 2020. Stripper Modification of a Standard MEA Process for Heat Integration with a Pulp Mill. <urn:nbn:se:kth:diva-289162>
- Ayittey, F.K., Obek, C.A., Saptoro, A., Perumal, K., Wong, M.K., 2020. Process modifications for a hot potassium carbonate-based CO<sub>2</sub> capture system: a comparative study. *Greenh. Gases Sci. Technol.* 10, 130–146. <https://doi.org/10.1002/ghg.1953>
- Barlow, H., S M Shahi, S., Loughrey, M., 2023. State of the Art: CCS Technologies 2023 [WWW Document]. Glob. CCS Inst. URL <https://www.globalccsinstitute.com/resources/publications-reports-research/state-of-the-art-ccs-technologies-2023>
- Bastarrica Anselmi, F., Camacho, M., Di Lavello, G., Iglesias Rossini, G., 2023. FERTILIZANTES VERDES EN URUGUAY [WWW Document]. World Energy Counc. URL <https://www.worldenergy.org/world-energy-community/future-energy-leaders>
- Bergman, H., 2022. Carbon capture in biomass combustion plants using promoted potassium carbonate solutions : A cost and safety evaluation. <urn:nbn:se:miun:diva-45253>
- Canada, N.R., 2015. Enzymatic Technology for Efficient Carbon Capture from Oil Sands Operations [WWW Document]. URL <https://natural-resources.canada.ca/science-and-data/funding-partnerships/funding-opportunities/current-investments/enzymatic-technology-for-efficient-carbon-capture-from-oil-sands-operations/16061>
- Emerson, E., 2010. White paper distillation column flooding [WWW Document]. URL [http://www.separationprocesses.com/Absorption/GA\\_Chp04a.htm](http://www.separationprocesses.com/Absorption/GA_Chp04a.htm)
- Errico, M., Madeddu, C., Pinna, D., Baratti, R., 2016. Model calibration for the carbon dioxide-amine absorption system. *Appl. Energy* 183, 958–968. <https://doi.org/10.1016/j.apenergy.2016.09.036>
- Fagerström, A., Grahn, D., Lundberg, S., Poulidikidou, S., Rydberg, T., Lewrén, A., Martin, M., Anderson, S., Hansson, J., Hjort, A., 2021. Large scale bio electro jet fuel production integration at CHP-plant in Östersund, Sweden. IVL Svenska Miljöinstitutet. <urn:nbn:se:ivl:diva-2772>
- Finance, Y., 2024. Industrial Carbon Dioxide Market Forecasted to Reach USD 7,177.6 Million by 2033, Growing at a CAGR of 3.2% | Exclusive Report by Persistence Market Research [WWW

Document]. Yahoo Finance. URL <https://finance.yahoo.com/news/industrial-carbon-dioxide-market-forecasted-141400334.html>

Fuji, T., 2022. Home [WWW Document]. Annex 58. URL <https://heatpumpingtechnologies.org/annex58/wpcontent/uploads/sites/70/2022/07/technologyfuji-electricsteam120.pdf>

Garcia, J.A., Villen-Guzman, M., Rodriguez-Maroto, J.M., Paz-Garcia, J.M., 2022. Technical analysis of CO<sub>2</sub> capture pathways and technologies. *J. Environ. Chem. Eng.* 10, 108470. <https://doi.org/10.1016/j.jece.2022.108470>

Genrup, M., 2023. Steam and Gas Turbines for Renewable Power Production - with Aero-engines - MVKN76.

Gustafsson, K., Sadegh-vaziri, R., Grönkvist, S., Levihn, F., Sundberg, C., 2021. BECCS with combined heat and power: assessing the energy penalty. *Int. J. Greenh. Gas Control* 110, 103434. <https://doi.org/10.1016/j.ijggc.2021.103434>

Hedström, J., 2014. Simulation and Assessment of Carbon Capture Processes Applied to a Pulp Mill. <https://hdl.handle.net/20.500.12380/200034>

Hikita, H., Asai, S., Tsuji, T., 1977. Absorption of sulfur dioxide into aqueous sodium hydroxide and sodium sulfite solutions. *AIChE J U. S.* 23:4. <https://doi.org/10.1002/aic.690230419>

Hoeger, C., Burt, S., Baxter, L., 2021. Cryogenic Carbon Capture™ Technoeconomic Analysis. SSRN Electron. J. <https://doi.org/10.2139/ssrn.3820158>

Hu, G., Nicholas, N.J., Smith, K.H., Mumford, K.A., Kentish, S.E., Stevens, G.W., 2016. Carbon dioxide absorption into promoted potassium carbonate solutions: A review. *Int. J. Greenh. Gas Control* 53, 28–40. <https://doi.org/10.1016/j.ijggc.2016.07.020>

Hurtado, J., 2023. Towards carbon neutrality: The top 10 global carbon capture projects of 2023 - PreScouter - Custom Intelligence from a Global Network of Experts. URL <https://www.prescouter.com/2023/10/carbon-capture-projects/>

IEA, 2023a. Emissions Industry [WWW Document]. IEA. URL <https://www.iea.org/energy-system/industry>

IEA, 2023b. Pulp & paper [WWW Document]. IEA. URL <https://www.iea.org/energy-system/industry/paper>

IEA, 2020. CCUS in the transition to net-zero emissions – CCUS in Clean Energy Transitions – Analysis [WWW Document]. IEA. URL <https://www.iea.org/reports/ccus-in-clean-energy-transitions/ccus-in-the-transition-to-net-zero-emissions>

IEA, 2019. Putting CO<sub>2</sub> to Use – Analysis [WWW Document]. IEA. URL <https://www.iea.org/reports/putting-co2-to-use>

IPCC, 2022. Mitigation Pathways Compatible with 1.5°C in the Context of Sustainable Development. pp. 93–174. <https://doi.org/10.1017/9781009157940.004>

- Jang, J.-K., 2016. Amines as occupational hazards for visual disturbance. *Ind. Health* 54, 101–115. <https://doi.org/10.2486/indhealth.2015-0071>
- Jiang, J., Hu, B., Wang, R.Z., Deng, N., Cao, F., Wang, C.-C., 2022. A review and perspective on industry high-temperature heat pumps. *Renew. Sustain. Energy Rev.* 161, 112106. <https://doi.org/10.1016/j.rser.2022.112106>
- Karlsson, H.K., Makhool, H., Karlsson, M., Svensson, H., 2021. Chemical absorption of carbon dioxide in non-aqueous systems using the amine 2-amino-2-methyl-1-propanol in dimethyl sulfoxide and N-methyl-2-pyrrolidone. *Sep. Purif. Technol.* 256, 117789. <https://doi.org/10.1016/j.seppur.2020.117789>
- Karthikeyan, T.L., 2020. Investigation of the absorption solvent for bioenergy carbon capture and storage (BECCS) through pilot plant trials. <urn:nbn:se:kth:diva-289165>
- Kearns, D., Liu, H., Consoli, C., 2021. TECHNOLOGY READINESS AND COSTS OF CCS. Klute, S., Budt, M., van Beek, M., Doetsch, C., 2024. Steam generating heat pumps – Overview, classification, economics, and basic modeling principles. *Energy Convers. Manag.* 299, 117882. <https://doi.org/10.1016/j.enconman.2023.117882>
- Koundinya, S., Jothilingam, J., Seshadri, S., 2023. Low-pressure steam generating heat pump – A design and field implementation case study. *Therm. Sci. Eng. Prog.* 45, 102140. <https://doi.org/10.1016/j.tsep.2023.102140>
- Kucka, L., Müller, I., Kenig, E.Y., Górak, A., 2003. On the modelling and simulation of sour gas absorption by aqueous amine solutions. *Chem. Eng. Sci.* 58, 3571–3578. [https://doi.org/10.1016/S0009-2509\(03\)00255-0](https://doi.org/10.1016/S0009-2509(03)00255-0)
- Kuparinen, K., Vakkilainen, E., Tynjälä, T., 2019. Biomass-based carbon capture and utilization in kraft pulpmills. *Mitig. Adapt. Strateg. Glob. Change* 24, 1213–1230. <https://doi.org/10.1007/s11027-018-9833-9>
- Kvamsdal, †, Rochelle, G., 2008. Effects of the Temperature Bulge in CO<sub>2</sub> Absorption from Flue Gas by Aqueous Monoethanolamine. *Ind. Eng. Chem. Res.* 47. <https://doi.org/10.1021/ie061651s>
- lab-ndt, 2014. LBNiW | Reference Project — Montes del Plata Pulp Mill 2012-2014. LBNiW. URL <https://lbniw.com/en/portfolio-items/montes-del-plata-pulp-mill-uruguay-2012-2014>
- Levihn, F., Linde, L., Gustafsson, K., Dahlen, E., 2019. Introducing BECCS through HPC to the research agenda: The case of combined heat and power in Stockholm. *Energy Rep.* 5, 1381–1389. <https://doi.org/10.1016/j.egy.2019.09.018>
- Li B.H., Zhang N., Smith R., 2014. Rate-based modelling of co<sub>2</sub> capture process by reactive absorption with mea. *Chem. Eng. Trans.* 39, 13–18. <https://doi.org/10.3303/CET1439003>
- Liao, Q., Liu, W., Meng, Z., 2022. Strategies for overcoming the limitations of enzymatic carbon dioxide reduction. *Biotechnol. Adv.* 60, 108024. <https://doi.org/10.1016/j.biotechadv.2022.108024>

Madeddu, C., 2018. MODELING AND ANALYSIS OF THE CO<sub>2</sub> POST-COMBUSTION CAPTURE PROCESS WITH MEA (PHD DEGREE). Università degli Studi di Cagliari.

Madeddu, C., Errico, M., Baratti, R., 2019. CO<sub>2</sub> Capture by Reactive Absorption-Stripping: Modeling, Analysis and Design, SpringerBriefs in Energy. Springer International Publishing, Cham. <https://doi.org/10.1007/978-3-030-04579-1>

Meldon, J.H., 2011. Amine screening for flue gas CO<sub>2</sub> capture at coal-fired power plants: Should the heat of desorption be high, low or in between? *Curr. Opin. Chem. Eng.*, Open issue 1/1 1, 55–63. <https://doi.org/10.1016/j.coche.2011.08.006>

MIEM, 2022. Green Hydrogen Roadmap in Uruguay [WWW Document]. Minist. Ind. Energ. Min. URL <https://www.gub.uy/ministerio-industria-energia-mineria/comunicacion/noticias/green-hydrogen-roadmap-in-uruguay>

Mokhatab, S., Poe, W.A., Mak, J.Y., 2019. Chapter 7 - Natural Gas Treating, in: Mokhatab, S., Poe, W.A., Mak, J.Y. (Eds.), *Handbook of Natural Gas Transmission and Processing (Fourth Edition)*. Gulf Professional Publishing, pp. 231–269. <https://doi.org/10.1016/B978-0-12-815817-3.00007-1>

Navedkhan, M., Lakshminarayan, J., Biliyok, C., Levihn, F., 2022. Integration of Hot Potassium Carbonate CO<sub>2</sub> Capture Process to a Combined Heat and Power Plant at Värtaverket. <https://doi.org/10.2139/ssrn.4286271>

Nilsson, F., 2023. Evaluation of Excess Heat Driven Carbon Capture Integrated at a Swedish Pulp Mill.

Novozymes, 2023. Carbon capture [WWW Document]. URL <https://www.novozymes.com/en/solutions/carbon-capture>

Numer Analytics, 2023. Overview of Wood Pulp. *Numer Anal.* URL <https://numeraanalytics.com/overview-wood-pulp>

Parkhi, A., Young, D., Cremaschi, S., Jiang, Z., 2023. Carbon dioxide capture from the Kraft mill limekiln: process and techno-economic analysis. *Discov. Chem. Eng.* 3, 8. <https://doi.org/10.1007/s43938-023-00024-7>

Pedersén, A., Larsson, A., 2017. Energy Efficiency Study at a Softwood Kraft Pulp Mill.

Peu, S.D., Das, A., Hossain, M.S., Akanda, M.A.M., Akanda, M.M.H., Rahman, M., Miah, M.N., Das, B.K., Islam, A.R.M.T., Salah, M.M., 2023. A Comprehensive Review on Recent Advancements in Absorption-Based Post Combustion Carbon Capture Technologies to Obtain a Sustainable Energy Sector with Clean Environment. *Sustainability* 15, 5827. <https://doi.org/10.3390/su15075827>

Quinde, A., 2020. Chip considerations: papermaking processes start with wood chip quality [WWW Document]. *Pulp Pap. Can.* URL <https://www.pulpandpapercanada.com/chip-considerations-papermaking-processes-start-with-wood-chip-quality>

Ramesh, K., Aziz, N., Shukor, S.R., Ramasamy, M., 2007. Dynamic Rate-Based and Equilibrium Model Approaches for Continuous Tray Distillation Column.

Razali, M.N., Jemaat, Z., Yunus, R., 2009. MONOETHANOLAMINE (MEA) WASTEWATER TREATMENT VIA CHITOSAN BASED ADSORPTION: A PRELIMINARY STUDY.

Razi, N., Svendsen, H.F., Bolland, O., 2013. Validation of mass transfer correlations for CO<sub>2</sub> absorption with MEA using pilot data. *Int. J. Greenh. Gas Control* 19, 478–491. <https://doi.org/10.1016/j.jggc.2013.10.006>

Regufe, M.J., Pereira, A., Ferreira, A.F.P., Ribeiro, A.M., Rodrigues, A.E., 2021. Current Developments of Carbon Capture Storage and/or Utilization—Looking for Net-Zero Emissions Defined in the Paris Agreement. *Energies* 14, 2406. <https://doi.org/10.3390/en14092406>

Robano E, Nuorimaa A., 2023. Project 2 of Biomass Conversion Course.

Sadeghalvad, B., Ebrahimi, H., Azadmehr, A., 2022. Chapter 3 - CO<sub>2</sub> capture by adsorption, in: Khalid, M., Dharaskar, S.A., Sillanpää, M., Siddiqui, H. (Eds.), *Emerging Carbon Capture Technologies*. Elsevier, pp. 63–89. <https://doi.org/10.1016/B978-0-323-89782-2.00012-0>

Salvador Palacios, N., 2023. Process and techno-economic analysis of a compact CO<sub>2</sub> capture technology.

Siemens, 2023. Heat pumps [WWW Document]. URL <https://www.siemens-energy.com/global/en/home/products-services/product-offerings/heat-pumps.html>, <https://www.siemens-energy.com/global/en/home/products-services/product-offerings/heat-pumps.html>

Skoglund, H., Fu, C., Harvey, S., Svensson, E., 2023. Integration of carbon capture in a pulp mill—effect of strategic development towards better biomass resource utilization. *Front. Therm. Eng.* 3. Stipanovic, A., 2023. Entrevista del 14 de junio de 2023: Alejandro Stipanovic - Radiomundo En Perspectiva [WWW Document]. URL <https://enperspectiva.uy/enperspectiva-uy/transcripciones/entrevista-del-14-de-junio-de-2023-alejandro-stipanovic>

Subramani, A., 2022. Techno-Economic Assessment of a Post-Combustion CO<sub>2</sub> Capture Unit in SCA Östrand Pulp Mill.

Svensson, E., Wiertzema, H., Harvey, S., 2021. Potential for Negative Emissions by Carbon Capture and Storage From a Novel Electric Plasma Calcination Process for Pulp and Paper Mills. *Front. Clim.* 3.

Svensson, H., 2023. CO<sub>2</sub> Capture, Storage, Utilization.

TAPPI, 2019. TAPPI Conference Papers. [WWW Document]. URL <https://www.Tappi.org/publications-standards/Tappi-conference-papers>

Technology, A., 2018. Rate-Based Model of the CO<sub>2</sub> Capture Process by MEA using Aspen Plus.

Tellgren, E., 2021. Växjö Energi first to test new carbon capture technology [WWW Document]. [www.veab.se](http://www.veab.se). URL <https://www.veab.se/om-oss/press/pressmeddelanden/2021/vaxjo-energi-forst-ut-med-att-testa-ny-teknik-for-att-fanga-in-koldioxid2>

Tobiesen, F.A., Juliussen, O., Svendsen, H.F., 2008. Experimental validation of a rigorous desorber model for CO<sub>2</sub> post-combustion capture. *Chem. Eng. Sci.* 63, 2641–2656. <https://doi.org/10.1016/j.ces.2008.02.011>

Tontiwachwuthikul, P., Meisen, A., Lim, C.J., 1992. CO<sub>2</sub> absorption by NaOH, monoethanolamine and 2-amino-2-methyl-1-propanol solutions in a packed column. *Chem. Eng. Sci.* 47, 381–390. [https://doi.org/10.1016/0009-2509\(92\)80028-B](https://doi.org/10.1016/0009-2509(92)80028-B)

Uruguay XXI, 2023. Chilean company to invest millions in Uruguay to produce eFuels from green hydrogen - News [WWW Document]. XXI. URL <https://www.uruguayxxi.gub.uy/en/news/article/compania-chilena-concretara-millonaria-inversion-en-uruguay-para-producir-ecombustibles-a-partir-de-hidrogeno-verde>

Vukasovic, V., Messina, D., 2023. Analisis-de-la-disponibilidad-de-CO<sub>2</sub>-H<sub>2</sub>V-Uruguay.pdf [WWW Document]. H2LAC. URL <https://h2lac.org>

Wang, N., Wang, D., Krook-Riekkola, A., Ji, X., 2023. MEA-based CO<sub>2</sub> capture: a study focuses on MEA concentrations and process parameters. *Front. Energy Res.* 11, 1230743. <https://doi.org/10.3389/fenrg.2023.1230743>

Warudkar, S.S., Cox, K.R., Wong, M.S., Hirasaki, G.J., 2013. Influence of stripper operating parameters on the performance of amine absorption systems for post-combustion carbon capture: Part I. High pressure strippers. *Int. J. Greenh. Gas Control* 16, 342–350. <https://doi.org/10.1016/j.ijggc.2013.01.050>

Zhou, S., Wang, S., Chen, C., 2012. Thermal Degradation of Monoethanolamine in CO<sub>2</sub> Capture with Acidic Impurities in Flue Gas. *Ind. Eng. Chem. Res.* 51, 2539–2547. <https://doi.org/10.1021/ie202214y>